Thrombospondin 2 (TSP2) Mitigates Abdominal Aortic Aneurysm via Modulating Extracellular Matrix Remodeling

Lanting Hu[1, 2†], Li Yin[1†], Yongli Ji[3†], Naiji Yu[4], Jianing Yue[5], Kaijie Zhang[1], Hongzhang Mei[6] , Yunlu Chen[7], Jinyi Chen[1], Weiwei Zhang[1,2], Kai Cao[1,2], Hanlei Zhou[1], Cuiping Xie[8], Yunxia Gong[1], Lihong Chen[2], Liya Lin[2], Da Huang[9], Maryam Maleki Goli[10], Parnia Ghanad[10] , Jian Shen[11,12,13*], Lu Zhao[14], Bowen Wang[6 *], Zhenjie Liu[1,2,15*]

[1] Department of Vascular Surgery, The Second Affiliated Hospital, School of Medicine, Zhejiang University, Hangzhou 310009, China.

[2] Research Center for Life Science and Human Health, Binjiang Institute of Zhejiang University, Hangzhou, 310053, China.

[3] The Department of Endocrinology, The Second Affiliated Hospital, School of Medicine, Zhejiang University, Hangzhou 310009, China.

[4] State Key Laboratory of Ophthalmology, Zhongshan Ophthalmic Center, Sun Yat-Sen University, Guangzhou 510060, China.

[5] Institute of Vascular Surgery, Department of Vascular Surgery, Zhongshan Hospital, Fudan University, 180 Fenglin Road, Shanghai 200032, China.

[6] Department of Surgery, School of Medicine, Northwestern University, Chicago, IL60603, USA.

[7] Center of Basic and Translational Research, The Second Affiliated Hosptital, Zhejiang University School of Medicine, Hangzhou 310009, China.

[8] The General ICU, the Second Affiliated Hospital of Zhejiang University School of Medicine, Hangzhou 310009, China.

[9] Department of Gynecology, The Second Affiliated Hospital of Zhejiang University School of Medicine, Hangzhou 310009, China.

[10] Zhejiang university, school of Medicine, Hangzhou 310058, China.

[11] Department of Cardiology, The Second Affiliated Hospital, School of Medicine, Zhejiang University, Hangzhou 310009, China.

[12] State Key Laboratory of Transvascular Implantation Devices, Hangzhou 310009, China.

[13] Heart Regeneration and Repair Key Laboratory of Zhejiang province, Hangzhou 310009, China.

[14] College of Pharmaceutical Sciences, Zhejiang University, Hangzhou 310058, China.

[15] Key Laboratory of Multiple Organ Failure (Zhejiang University), Ministry of Education, Hangzhou 310058, China.

† The first three authors contributed equally to the study.

*Corresponding authors: Zhenjie Liu (Tel: +86 15268135830, email: lawson4001@zju.edu.cn), Bowen Wang (email: bowenwang@northwestern.edu) and Jian Shen (email: shenjian27753@zju.edu.cn).

Zhenjie Liu is the lead corresponding author.

Running Title: TSP2 Preserves Aortic ECM Integrity in AAA

Highlights：

TSP2 is predominantly expressed by adventitial fibroblasts in AAA.

TSP2 deficiency accelerates AAA progression via ECM disorganization.

Akt/STAT3 signaling drives TSP2 transcription in fibroblasts.

Local TSP2 delivery rescues ECM integrity and mitigates AAA in a murine model

Abstract

Abdominal aortic aneurysm (AAA) is a lethal yet prevalent vascular disease, featuring progressive extracellular matrix (ECM) degradation and aortic dilation. Despite its high mortality upon rupture, there are still no medical treatments with proven benefits for AAA. In the current study, we identified thrombospondin-2 (TSP2) as a critical modulator against ECM degradation in AAA. Utilizing specimens from patients undergoing open AAA repairs, we observed that both aortic and circulating TSP2 levels were significantly upregulated and positively correlated with aortic wall thickness. Single-cell RNA sequencing and immunofluorescence staining further localized TSP2 primarily to adventitial fibroblasts. Using transgenic whole-body knockout mice, TSP2 deletion accelerated elastase-induced AAA growth, heightened rupture incidence, and exacerbated collagen loss and elastin disruption. Conversely, lentivirus-mediated TSP2 re-introduction in whole-body knockout mice effectively rescued ECM integrity and aortic homeostasis. Mechanistically, chromatin-immunoprecipitation and gain-/loss-of-function studies identified Akt-dependent phosphorylation of STAT3 as a direct transcriptional driver of TSP2. Therapeutically, local delivery of exogenous TSP2 via peri-aortic hydrogel effectively mitigated ECM destruction and AAA formation. Collectively, our current study study established TSP2 as a fibroblast-derived stabilizer of vascular ECM and highlighted its therapeutic potential for AAA through targeted modulation of matrix remodeling pathways.

Keywords: Abdominal aortic aneurysm, Thrombospondin-2, Extracellular matrix remodeling, Adventitial fibroblasts, Akt/STAT3 signaling

Introduction

Abdominal aortic aneurysm (AAA) is a life-threatening condition characterized by the progressive dilation of the abdominal aorta [1]. Its prevalence escalates markedly with age, affecting 5-10% of men over 65 years [4]. Despite exhibiting lower incidence of AAA in comparison to male, female patients tend to experience more rapid aneurysm growth and a higher risk of rupture [5 6]. The progressive weakening of aortic wall and the gradual expansion of the aneurysmal sac could culminate in rupture, resulting in hemorrhagic shock and high mortality [7]. Surgical repairs – open surgery and endovascular repair (EVAR) – remain the standard treatments for AAAs larger than 5.5 cm, while elective surgeries for smaller, asymptomatic AAAs are not indicated [8]. Despite decades of active clinical trials, there remains a lack of effective pharmacotherapies to halt the progression of diagnosed AAAs [9]; instead, small, asymptomatic AAAs are usually managed through a "watchful waiting" approach/strategy [10]. Moreover, the size of AAA does not reliably predict the risk of rupture [11] [12], and it remains an unmet medical need to develop robust biomarker(s) that can faithfully inform the rate of AAA progression and its lethal rupture[9]. Understanding the underlying mechanisms driving AAA progression and identifying therapeutic targets that can halt or reverse this process remains critical.

Central to AAA pathogenesis is the dysregulation of extracellular matrix (ECM) homeostasis [13]. ECM remodeling, including the degradation of key proteins like collagen and elastin, weakens the aortic wall, contributing to AAA expansion and rupture [14]. While ECM remodeling is well-characterized in AAA, the regulatory proteins governing this process—particularly

those with dual roles in matrix stabilization and cellular signaling—remain incompletely understood. Among these, the thrombospondin (TSP) family has garnered significant attention for its roles in tissue repair, inflammation, and ECM remodeling[15].

The TSP glycoprotein family is comprised of 5 members (TSP1-5), withTSP1 and TSP2 being the most well-characterized isoforms in cardiovascular system. Despite of their structural similarities, tTSP1 and TSP2 exhibit distinct biological functions[16]. Our previous studies have shown that TSP1 exacerbates AAA progression by promoting inflammatory cell recruitment and enhancing ECM degradation[17] [18]. In contrast, despite recent proteomic endeavors, the mechanistic role and theranostic implications of TSP2 have yet to be elucidated. [19] [20]. Indeed, elevated TSP2 levels have been observed in AAA tissue [13] and patient plasma [21], yet it remains completely unknown as to TSP2's role as a protector or disease promoter of AAA..

Here, we aim to comprehensively interrogate TSP2's role in AAA pathogenesis. In a retrospective cohort study, TSP2 levels – both aortic and circulating – were consistently elevated in AAA patients and positively correlated with aortic diameter. Combining single-cell transcriptomics, genetic knockout mouse model, and targeted interventions, we demonstrate that TSP2, primarily derived from adventitial fibroblasts, safeguards aortic integrity by orchestrating adventitial collagen organization and elastin preservation. Mechanistically, TSP2 expression is governed by the Akt/STAT3 axis, linking mechanical stress to ECM homeostasis. Collectively, our findings establish the novel role of TSP2 as a protector against AAA pathogenesis.

Methods

Patient Materials and Ethics

The study complies with the Declaration of Helsinki for the ethical treatment of human specimens and was approved by the Human Research Ethics Committee of the Second Affiliated Hospital, School of Medicine, Zhejiang University (No.2016-085). Data and samples from AAA patients and healthy control were collected from June 2016 to July 2024. AAA patients' aortic samples were obtained from patients undergoing elective open repair of AAA, while patients with infectious or inflammatory aneurysms and pseudoaneurysms were excluded. Healthy control aortic samples were obtained from patients undergoing kidney transplantation for conditions unrelated to aortic diseases. Vessel samples underwent routine fixation, dehydration, embedding, and sectioning (5 μm) for subsequent analysis. All participants provided written informed consent prior to their participation and sample collection. Details of AAA patients are provided in table S1.

Measurement of Vascular Adventitia Thickness

For human CT imaging measurements, vascular adventitia thickness was measured along eight directions (0°, 45°, 90°, 135°, 180°, 225°, 270°, and 315°) on cross-sectional CT images of AAA patients, and the average thickness was calculated.

For mouse tissue section measurements, abdominal aortic tissues were collected at the experimental endpoint, fixed in 4% paraformaldehyde, embedded in paraffin, and serially

sectioned at 5 μm thickness. H&E staining was performed to visualize the adventitial structure, and ImageJ software was used to measure adventitia thickness at multiple locations, with the average value calculated. Adventitia thickness was defined as the distance from the external elastic lamina to the outermost layer of the vascular adventitia. At least five cross-sections (CT) or five histological sections per sample were analyzed, and the final mean adventitia thickness was determined.

Mice

For the sake of readability and clarity, this paper will refer to both TSP2 and *Thbs2* (the gene encoding the TSP2 protein) as TSP2, despite one being a protein and the other a gene.

All animal husbandry and experiments were approved by the Laboratory Animal Ethics Committee of the Second Affiliated Hospital, School of Medicine, Zhejiang University (No. 2022-087). All procedures conformed to the Directive 2010/63/EU of the European Parliament and the current NIH guidelines for the protection of animals used for scientific purposes. Given that AAA predominantly occurs in males in humans, only male mice were used in this study. TSP2 $^{-/-}$ and ApoE $^{-/-}$ mice with a C57BL/6J genetic background were purchased from GemPharmatech Co., Ltd (Jiangsu). C57BL/6J mice were obtained from Charles River (Zhejiang). To generate ApoE $^{-/-}$ TSP2 $^{-/-}$ mice, ApoE$^{-/-}$ mice were crossed with TSP2$^{-/-}$ mice to produce ApoE $^{+/-}$ TSP2 $^{+/-}$mice, which were backcrossed with ApoE $^{-/-}$ mice to generate ApoE $^{-/-}$ TSP2 $^{+/-}$ mice. These mice were then intercrossed to generate ApoE $^{-/-}$ TSP2 $^{-/-}$ mice.All mice were housed under controlled light/dark conditions (12-hour light/12-hour dark cycle), in

temperature-regulated and pathogen-free facilities, with unrestricted access to clean food and water. The mice in different groups were not from the same parents, but they were all in C57BL/6J genetic background. In addition, sex- and age-matched animals were used for each study. Therefore, the genetic variations among groups are likely to be minimal and not affect the conclusions. To reduce selection bias, mice were assigned to experimental groups using randomization. During data collection and analysis, researchers were blinded to group allocation. The number of animals used in this study was determined using the "resource equation" method [22]. According to this method, the degree of freedom for analysis of variance (ANOVA) is calculated as E = Total number of animals − Total number of groups. The animal numbers were adjusted to ensure that the value of E remained between 10 and 20, as this range is considered sufficient to detect meaningful differences while avoiding unnecessary animal use.

Murine Models of AAA

Mice were anesthetized using stepwise isoflurane inhalation anesthesia, initiated with 5% isoflurane for induction and maintained with 1.5–2% isoflurane during the surgical procedure. Isoflurane (R510-22, RWD, Shenzhen, China) was delivered via an anesthesia machine with oxygen (1 L/min) as the carrier gas. All surgical procedures were performed under a stereomicroscope (Carl Zeiss, USA). Animals were under constant physiological monitoring during surgery.

The postoperative analgesia protocol included: an subcutaneous injection of buprenorphine

(0.05 mg/kg; PHR1729, Sigma-Aldrich, USA) and meloxicam (5 mg/kg; H20250012, Delova Bio, Nanjing, China) immediately after surgery, followed by topical application of 2.5% lidocaine ointment (H20063466, Tongfang Pharmaceutical Group Co. Ltd., China) to the incision site. Subcutaneous buprenorphine (0.05 mg/kg) is administered every 12 hours during the first 48 postoperative hours, and meloxicam (5 mg/kg) is given every 24 hours until 72 hours after surgery. All pharmaceutical products to be verified for batch validity prior to administration.

At designated time points, mice were euthanized in accordance with the AVMA Guidelines for the Euthanasia of Animals (2020 edition). Animals were placed in an induction chamber and exposed to 5% isoflurane in oxygen (1 L/min) for at least 5 minutes until loss of consciousness (absence of righting reflex). Subsequently, a secondary physical method (cervical dislocation) was performed to ensure death. Following euthanasia, transcardial perfusion with 4% paraformaldehyde (PFA) was performed for tissue fixation.

For animals that died unexpectedly during the experiment, necropsies were performed, and the formation of periaortic hematomas was used as the criterion for diagnosing ruptured abdominal aortic aneurysms.

Elastase model: The elastase-induced AAA model was established as previously described [23]. A midline abdominal incision was made to expose the infrarenal aorta up to the bifurcation. The abdominal aorta was then carefully dissected from the inferior vena cava and freed from below the left renal vein to the bifurcation. The lumbar artery branches were ligated using 10-0 nylon sutures, and the proximal and distal ends of the aorta were ligated to block blood flow. A 30G needle was used to puncture and ligate the distal aorta, with a microcatheter inserted

and secured at the puncture site using sutures. After flushing the aorta with 37°C saline to remove any residual blood, a pre-prepared solution of porcine pancreatic elastase (PPE, 4.5 U/mL, HY-P2974, MedChemExpress, NJ) was infused under 110 mmHg (1 mmHg=0.133 Kpa) pressure for 10 minutes. The microcatheter was then removed, and the puncture site was sutured with 11-0 nylon sutures. The distal aortic block was released, followed by the opening of the proximal aortic block. Hemostasis was applied to the puncture site as needed. The abdominal wall and skin were sutured layer by layer with 6-0 absorbable sutures. On postoperative day 14, AAA specimens were collected from the mice.

Angiotensin II (Ang II) model: Ang II-induced AAA model was established as described in reference [24]. Ang II (1000 ng/kg/min, Sigma-Aldrich, MO) was infused using a subcutaneously implanted osmotic pump (Model 2004, ALZET, Cupertino, CA) for 28 days in *ApoE* $^{-/-}$ mice to induce AAA formation. The mice were fed a western diet (high fat and cholesterol diet, D12109C, SiPeiFu, Beijing), 3 weeks prior and maintained to Ang II infusion. On postoperative day 28, AAA specimens were collected from the mice.

CaPO4 model: The CaPO4-induced AAA model was established using a method similar to the CaCl2-induced AAA model [25]. Under general anesthesia, a midline incision was made to expose the infrarenal region of the abdominal aorta. A small piece of gauze soaked in 1 mol/L CaCl2 solution was applied perivascularly for 10 minutes. This was followed by a 5-minute treatment with PBS solution. The abdominal wall and skin were sutured layer by layer. AAA specimens were collected from the mice on postoperative days 1, 3, 7, 10, and 14.

Ultrasonography

Mice were initially anesthetized using 5% isoflurane. After animals were sedated, anesthesia was maintained by 1% to 2% isoflurane during the examination. Aortic measurements were performed using the Vevo 3100 imaging system (FUJIFILM VisualSonics, Tokyo). We took longitudinal view of abdominal aorta for measurements. B-mode ultrasound was used to identify aorta. Color spectral Doppler was then used to verify that the direction and velocity of blood flow were consistent with an aortic signal. The maximum external diameter of the infrarenal aorta was measured prior to treatment (initial measurement) and at the time of tissue harvest (final measurement). Aortic expansion (% aortic dilation) was determined by aortic expansion relative to pre-treatment diameter ((Final measurement – initial measurement)/Initial measurement)*100%. Aneurysm was defined as a 50% increase in aortic diameter.

Tissue collection and disposal

Human blood samples were collected via venipuncture, while mice blood samples were obtained through tail vein bleeding. Blood samples were collected into sodium citrate-coated tubes and centrifuged at 4,000 × g for 15 minutes to obtain platelet-poor plasma which was stored at -80°C. After perfusion with sterile PBS, the mouse aortas were processed as follows: some samples were immediately embedded in OCT compound for frozen sectioning at 7 μm thickness; the remaining samples were additionally perfused with 4% paraformaldehyde for fixation, then embedded in paraffin and sectioned at 5 μm thickness for hematoxylin and eosin (H&E) staining, Masson's trichrome staining, Verhoeff-Van Gieson

(VVG) staining, immunofluorescence staining, or subsequent biochemical analyses.

Immunohistochemistry (IHC)

After deparaffinization and antigen retrieval, aortic sections were washed with PBS once and immersed in 3% H_2O_2 for 10 minutes, then blocked with 5% normal goat serum (NGS) for 1 hour. Sections were incubated overnight at 4 °C with primary antibodies (Table S2) or corresponding normal IgG (negative control). After washing with PBS, sections were incubated with horseradish peroxidase (HRP)–conjugated goat anti-rabbit IgG polyclonal antibodies for 23 minutes. Sections were developed with DAB substrate, counterstained with hematoxylin, and mounted. All section images were captured with a light microscope (DM2500, Leica, Wetzlar).

Immunofluorescent staining（IF）

Antigen retrieved sections underwent PBS washing and were permeabilized along with blocking with 0.05% Triton X-100, 0.5% bovine serum albumin (BSA) and 5% NGS in PBS for 1 hour. Primary antibodies (Table S2) were incubated overnight at 4 °C. The following day, secondary antibodies conjugated with Alexa Fluor 488/555 were applied for 1 hour at room temperature. Sections were mounted with Fluoromount-G™ antifade reagent with DAPI (36308ES, Yeasen, Shanghai) and imaged with a fluorescence microscope (DM6B, Leica).

Immunocytochemistry（ICC）

NIH3T3 fibroblasts were fixed with 4% paraformaldehyde for 10 minutes, permeabilized with 0.1% Triton X-100 for 10 minutes, and then blocked with 5% bovine serum albumin (BSA) for

1 hour at room temperature. Cells were incubated with primary antibodies (Table S2) overnight at 4°C, followed by secondary antibody incubation for 1 hour at room temperature. Cells were mounted using Fluoromount-G™ antifade reagent containing DAPI (36308ES, Yeasen, Shanghai) and imaged using a fluorescence microscope (DM6B, Leica).

Histology

Elastic staining and modified Masson staining were performed according to the manufacturers' protocols using corresponding assay kits (HT25A, Sigma-Aldrich, MO and G1346, Solarbio, Beijing). Images were captured using a Leica DM2500 microscope.

Pathological Scoring: Elastin degradation in the aortas was blindly assessed using the following scoring system: score 1 (< 25), score 2 (25% –50%), score 3 (50%–75%), score 4 (>75%). Discontinuous sections in the middle part of each infused area with 20 μm intervals over a total span of 100 μm (every 4th section for a total of 5 sections) were analyzed. The mean score of these sections represented the overall elastin degradation level for each sample.

Collagen Quantification: Collagen content in Masson-stained sections was quantified using ImageJ FIJI software (NIH, USA). Images were converted to grayscale, and a threshold was applied to distinguish collagen-rich regions. The collagen area was expressed as a percentage of the total tissue area. Five sections from each sample, taken as described above, were used for collagen content quantification, and the average value was calculated.

Transmission Electronic Microscopy (TEM)

After fixing in 2.5% glutaraldehyde in a 0.1 M phosphate buffer for 4 h at RT and overnight at

4 ◦C, mouse abdominal aorta tissues were fixed with 1% OsO4 and washed with ddH2O, followed by dehydration with graded alcohol and embedding in acetone, acetone with 33% epoxy resin, and epoxy resin successively. Ultrathin sections (50 nm) were cut by a Leica UC7 slicer and placed on copper grids, stained with uranyl acetate and lead citrate, and examined under a 120 kV electron microscope (Talos L120C, Thermo Scientific, USA).

ELISA

TSP2 levels were measured via a Human Thrombospondin-2 ELISA Kit (EH452RB, Thermo Fisher, MA). In brief, plasma samples and standards were pipetted into TSP2 antibody-coated wells. After washing, biotin-linked TSP2 antibody and HRP-conjugated streptavidin were applied for signal magnification. The reaction was visualized with TMB substrate, followed by a stop solution, and absorbance was measured at 450 nm.

Cell culture

The murine macrophage cell line RAW264.7, murine fibroblasts cell line NIH3T3, human endothelial cells line HUVEC and human aorta smooth muscle cells line T/G HA-VSMC was obtained from American Type Culture Collection (ATCC, Manassas, VA). Primary human aortic adventitial fibroblasts were purchased from Procell (Pricella Biotechnology Co., Ltd, Wuhan). Cells were cultured according to the manufacturer instructions. Bone marrow-derived macrophages (BMDM) were isolated from bone marrow of the femur and tibia of C57BL/6J mice. Cells were cultured in RPMI-1640 medium supplemented with 10% FBS, mouse M-CSF recombinant protein (50 ng/ml, eBioscience, Waltham, MA) for 5-7 days [26]. Aortic adventitial

fibroblasts (AFs) were isolated from the adventitial layer of the aorta of C57BL/6J mice. After euthanizing the mice, the aorta was excised, and the adventitial layer was separated. The tissue was digested with collagenase and DNase in RPMI-1640 medium for 30-60 minutes. The cell suspension was filtered, centrifuged, and resuspended in RPMI-1640 medium containing 10% FBS and 1% penicillin-streptomycin for culture.

The in vitro cellular pathology models were established as follows: (1) For the Ang II stimulation model, cells were treated with complete medium containing 1 μM angiotensin II (Ang II, HY-13948, MedChemExpress) for 24 hours before subsequent experiments; (2) For the calcification induction model, cells were first washed twice with 1× PBS buffer, then incubated with 0.05 M $CaCl_2$ in 1× PBS solution (where Ca^{2+} reacts with phosphate to form $CaPO_4$ precipitates) at 37°C for 15 minutes, after which the $CaCl_2$ solution was removed and cells were washed twice with DMEM containing 10% FBS before proceeding to subsequent steps[25]; (3) For the elastase digestion model, cells were washed twice with 1x PBS buffer, treated with 0.4 U/mL elastase (HY-P2974, MedChemExpress, NJ) solution at 37 °C for 5 minutes, and then washed again with 1x PBS buffer prior to further experimentation[27].

Transduction and transfection

Lentiviral vectors for TSP2 overexpression were purchased from Genechem Co., Ltd (Shanghai), where the CBh-gcGFP Gv492 plasmid, with or without (negative control) the short hairpin TSP2 expression sequence, was used. Fibroblasts were transduced at a multiplicity of infection (MOI) of 20 using HiTransG P (Genechem). Transfected cells were incubated for 48

hours before subsequent assays.

Expression plasmids for Flag-tagged STAT3 and the Y705E mutation (constitutively active STAT3) were based on those previously described [28]. In addition, plasmids encoding the dominant-negative (DN)-Akt and constitutively active myristoylated mutant Akt (MYR-Akt), which induced phosphorylation of Akt, were also based on previous descriptions[29] .

The fibroblasts were cultured in DMEM/F12 medium containing 10% FBS and 1× penicillin-streptomycin and maintained in a cell culture incubator at 37°C and 5% CO_2.

Antibiotics were removed 24 hours before transfection. When cells were grown in 6-well plates to 60–80% confluence for *TSP2* knockdown, 10 μL Lipofectamine RNAiMAX (13778, Thermo Fisher) was added into 250 μL Opti-MEM™ medium (31985, Thermo Fisher) and mixed with 250μL 50 nM siRNA (Table S3). The mixture was pipetted to the well with 1,500 μL Opti-MEMTM medium 20 minutes later for the following 8 hours transfection.

CCK8 assay

After cultured 24 hours with or without angiotensin II, 10μL WST-8(HY-K0301, MedChem Express) was added into 100μL medium for a 30~60 minutes incubation under 37°C. Absorbance was measured at 450 nm (OD_{450}) using a SpectraMax ABS plus spectrophotometer (Molecular Devices, CA).

Cell adhesion assay

The cell suspension was adjusted to 4 × 10^5 cells/ml. 100 µl of the cell suspension was added to each well of a pre-collagen-coated 96-well plate (152038, Thermo Fisher) and incubated at 37°C for 45 minutes. Non-adherent cells were washed off, and adherent cells were fixed with 4% paraformaldehyde for 3 minutes and stained with Crystal Violet (5 mg/ml in 2% ethanol, Sigma) for 10 minutes. Absorbance at 450 nm (OD_{450}) was then measured using a CCK8 assay kit (HY-K0301, MedChem Express). Five replicates were set for each group, and the mean value was calculated. Cell adhesion(%) = OD of the adhered cells/OD of the total cells×100%.

Cell contraction assay

The cell contraction assay was performed using the CytoSelect™ Cell Contraction Assay Kit (CBA-5020, Cell Biolabs, Inc., USA). Briefly, a cell suspension of 2×10^6 cells/mL was prepared and mixed with collagen gel solution at 4:1 ratio. 0.5 mL mixture was added to each well of a 24-well cell contraction plate and incubated at 37°C, 5% CO_2 for 1 hour. After collagen polymerization, 1 mL of medium (with or without Ang II) was added, and incubation continued for 1 day. Collagen gel area was measured using ImageJ FIJI software (NIH, USA).

Transwell migration assay

Macrophages RAW264.7 (4 × 10^5 cells) were seeded in 100 µL of high-glucose DMEM medium and loaded into 8-µm pore size transwells (3422, Corning NY), which were placed onto 24-well plates containing 350 µL of DMEM/F12 medium supplemented with 10% FBS.

These medium were collected from the human primary adventitial fibroblasts in the Control group, Ang II group, AngII+*TSP2*oe group and AngII+*TSP2*kd group. After 24 hours of incubation at 37 °C, cells in transwells were erased while migrated cells were fixed with paraformaldehyde, stained with crystal violet and captured with DMi1 microscope (Leica).

Chromatin immunoprecipitation (ChIP)-qPCR

ChIP assay was performed using SimpleChIP™ Enzymatic Chromatin IP Kit (#9003, Cell Signaling Technology, MA). In brief, NIH3T3 cells were crosslinked with 1% formaldehyde, and chromatin was digested using micrococcal nuclease. Following sonication, chromatin fragments were immunoprecipitated using specific antibodies and magnetic beads. After washing, crosslinks were reversed, and the DNA was purified using the provided reagents. Quantitative PCR (qPCR) was performed to analyze the enrichment of specific DNA sequences. Quantitative results are displayed as corresponding fold change. PCR products of immunoprecipitated and input samples were analyzed on a 1% agarose gel. Primers used for qPCR and ChIP assays are listed in Tables S2.

Southern blot (SB)

Prepare a 1% agarose gel by mixing 1g agarose with 100 mL freshly prepared 1× TBE buffer, heating until fully dissolved. Add 10 μL 4S GelRed nucleic acid stain (#A616697, Sangon Biotech, Shanghai) and mix thoroughly. Cast the gel, perform electrophoresis, and visualize the results using a UV transilluminator (Gel DocXR+ , Bio-RAD).

Western blot (WB)

Total protein was extracted by Total Protein Extraction Kits (BC3710, Solarbio, PRC). Protein concentration was measured by a Pierce™ BCA Protein Assay Kit (23227, Thermo Fisher Scientific, USA) and diluted with lysis buffer to equalization and the final resolution was mixed with loading buffer (P0015l, Beyotime, PRC). Equal amounts of protein were separated by electrophoresis on 4~20 % SDS PAGE Gels (ET12420Gel, ACE Biotechnology, PRC) and transferred to PVDF membranes (IPVH00010, Millipore, USA). Membranes were then blocked with Protein Free Rapid Blocking Buffer (PS108, YaMei, PRC) for 1 h and probed with primary antibodies at 4 ℃ overnight and secondary antibodies for 1h at room temperature. The blots were cut and separated into sections for different antibody probing (Table S2). Protein expression was detected in a chemiluminescence solution (BL520A, Biosharp, Beijing) by Chemiluminescence imaging system (ImageQuant^{TM} 800, Amersham, USA) and analyzed via densitometry with ImageLab software (v6.0, Bio-Rad, USA). The relative expression of a specific protein was calculated using the non-phosphorylated form or GAPDH as a reference, with protein levels normalized and expressed as a percentage of the reference.

RT-qPCR

Total RNA was extracted using Trizol reagent (15596026, Thermo Fisher) according to the manufacturer's protocol. RNA was then reverse-transcribed using HiScript III All-in-one RT SuperMix Perfect for qPCR (R333, Vazyme, Nanjing). Real-time PCR and data collection were conducted with ChamQ Universal SYBR qPCR Master Mix (Q711, Vazyme) on a 7500 Fast PCR instrument (Applied Biosystems™, Thermo Fisher). Relative expression levels were

normalized to α-tubulin, calculated using the $2^{-\Delta\Delta CT}$ method. The results are presented as fold changes relative to the control group average. Primers are listed in Table S3.

Release-controlled hydrogel preparation and application

Hydrogels were prepared as previously described, with SH-gel-5 used as the selected concentration [30].Prior to adding the initiator, the solution was sterilized by UV irradiation for 30 minutes. Subsequently, the appropriate amount of mouse TSP2 protein (HY-P702563, MedChemExpress, China) was added to achieve a concentration of 1 μg/mL. Following elastase perfusion to induce AAA in mice, about 20 μL hydrogel was gummed onto infused aorta topically and solidified by ultraviolet in situ for 65 seconds. The abdominal cavity was then closed. The control group received hydrogel without the addition of TSP2 protein.

Pluronic F-127 hydrogel preparation and application

Pluronic F-127 (Sigma-Aldrich, St. Louis, MO, USA) was prepared as a 30% (w/v) suspension in 0.1M phosphate-buffered saline (PBS, pH 7.6), shaken overnight at 4°C until fully dissolved, and stored at 4°C. Lentiviral vectors (KL63389-1, Genechem, Shanghai) were mixed with Pluronic F-127 on ice to achieve a final vector concentration of 4 × 10^8 TU/mL and a hydrogel concentration of 22%. All procedures were conducted under sterile conditions. After elastase perfusion, approximately 20 μL of hydrogel was applied to the perfused aorta. The control group was treated with negative control lentivirus (CON335, Genechem, Shanghai).

RNA-sequencing and data analysis

Single-cell sequencing data analysis： Datasets (GSE166676 and GSE152583) include single cell sequencing data from mouse and human AAA samples. Preprocessing, normalization, data scaling, and cell clustering were performed using Seurat (Version 5.0.3). For cluster identification, we used SingleR (v. 2.0.0) to determine specific cell populations. Subsequently, we assessed TSP2 expression across different cell types within these datasets.

Bulk RNA sequencing data analysis： Bulk RNA sequencing of human primary aortic adventitia fibroblasts was performed on an Illumina HiSeq2500 sequencer. DEGs were identified using DESeq2 (Version 1.40.2) with a fold change > 1.5 and adjusted p-value < 0.05. Subsequently, we used clusterProfiler (v. 4.8.3) and enrichplot (Version 1.20.3) to carry out Gene Ontology (GO) and Kyoto Encyclopedia of Genes and Genomes (KEGG) enrichment analyses on the DEGs.

Statistical analysis

All data were reported as mean ± standard error of the mean (SEM), and all statistical tests were two-tailed, where n represents the number of animals, different cell cultures, or patients studied, with data presented as dot plots (each point indicating an independent biological replicate). Statistical analyses were performed using GraphPad Prism Software (v10.2.3, San Diego, USA), with data distribution assessed by the Shapiro-Wilk test: normally distributed data used unpaired Student's t-test (two groups) and ordinary one-way ANOVA (≥3 groups), while non-normally distributed data (including ordinal categorical variables) used Mann-Whitney *U* test (two groups) or Kruskal-Wallis *H* test (≥3 groups), and survival analysis employed the log-rank (Mantel–Cox) test, with $p < 0.05$ considered statistically significant. The statistical analysis methods for both single-cell and bulk RNA-seq datasets are described above.

results

3.1. TSP2 is upregulated in human and experimental AAA.

To investigate the correlation between TSP2 and AAA, we retrospectively analyzed the aortic specimens, serum, and radiology data from 21 patients who underwent surgery for AAA. Utilizing computed tomography (CT) imaging, we observed significantly thickened aneurysm walls in AAA patients (Figure 1A). Circulating TSP2 levels were markedly elevated in AAA patients compared to age- and sex-matched healthy controls, and a positive correlation was observed between serum TSP2 levels and aneurysm wall thickness (Figure 1B, 1C). Consistent

with recent report, immunohistochemical (IHC) staining revealed significant elevation of TSP2 protein expression in AAA tissues in comparison to healthy control. Moreover, our data demonstrated that TSP2 expression was predominantly elevated in the adventitia of AAA tissues, with moderate increases in the media (Figure 1D).

To further explore the dynamic changes in TSP2 expression during AAA pathogenesis, we employed an experimental model of AAA via intraluminal perfusion with porcine pancreatic elastase. Western blot (WB) analysis confirmed significantly higher TSP2 protein levels in AAA tissues compared to sham controls (Figure 1E). Temporal profiling of TSP2 levels revealed that serum TSP2 concentrations peaked at Day 3 post-surgery and subsequently declined (Figure 1F). Similarly, TSP2 mRNA levels in AAA tissues showed a comparable pattern. Furthermore, IHC staining of elastase- perfusion-induced AAA mice and Angiotensin II (Ang II)-induced AAA mice further confirmed that TSP2 was significantly upregulated in the early stage of AAA and gradually declined thereafter (Figure 1G and supplementary Figure 1). These findings underscored the temporal regulation of TSP2 in AAA, particularly in the adventitia.

3.2. TSP2 deficiency exacerbates ECM degradation and AAA progression.

To interrogate the potential involvement of TSP2 in AAA pathogenesis, we induced experimental AAA lesions inin 8-week-old male $TSP2^{-/-}$ mice versus wild-type ($TSP2^{+/+}$) mice of C57bl6/j background by intraluminal perfusion with porcine pancreatic elastase as previously described. Fourteen days after surgery, color Doppler ultrasound revealed a 2.41±0.09 -fold enlargement of maximal aortic diameter without any incidence of ruptured AAA in the wild-type control, consistent with literature reports. In stark contrast, $TSP2^{-/-}$ mice displayed exacerbated aneurysmal growth (3.37±0.16 -fold) as well increased susceptibility to rupture in the abdominal aorta (Figure 2D, 2Eand Supplementary Figure 2).

Microscopically, hematoxylin and eosin (H&E) staining revealed profound aortic thickening in $TSP2^{-/-}$ mice, particularly in the adventitia (Figure 2E and F). Collagen and elastin are essential ECM proteins in the aortic wall, providing tensile strength and compliance, respectively [31] [32]. Quantitative analysis of collagen fibers from Masson-stained images showed a significant reduction in collagen fiber content in $TSP2^{-/-}$ mice compared to $TSP2^{+/+}$ mice (Figure 2G). Scoring of elastin fiber fragmentation from Verhoeff-Van Gieson (VVG) stained images indicated that $TSP2^{-/-}$ mice exhibited more fragmented and disorganized elastin fibers (Figure 2H).

Collagen in the vascular system mainly consists of type I and type III. Collagen I provides strength and structural support to the vessel, while Collagen III is essential for vascular elasticity and flexibility. Fibronectin, a glycoprotein present in the ECM, binds to integrin

receptors on the cell membrane, facilitating cell attachment to collagen and serving as a link between cells and the ECM [33]. IF staining of abdominal aortic tissue sections showed that Collagen I, Collagen III, and Fibronectin exhibited reduced fluorescence intensity and coverage in $TSP2^{-/-}$ mice compared to $TSP2^{+/+}$ mice (Figure 2I and 2K). The similar phenomenon was observed in human abdominal aortic (Figure 2J and 2L). However, the markers for T lymphocytes (CD3), B lymphocytes (CD19), and monocytes/macrophages (CD68) did not show significant differences between $TSP2^{+/+}$ and $TSP2^{-/-}$ mice (Supplementary Figure 3).

3.3. TSP2 is highly expressed in adventitial fibroblasts in AAA tissue

Next, we analyzed the cell-specific expression of TSP2 in publicly archived single-cell sequencing datasets of human and murine AAA obtained from the GEO database (GSE152583 and GSE166676). Following clustering and annotation as described previously, our analysis revealed that TSP2 is predominantly expressed by fibroblasts in AAA (Figures 3A and 3B). To corroborate our findings, we compared the endogenous expression level of TSP2 across multiple relevant cell types, including human primary culture of endothelial cells (HUVEC), macrophages (BMDM), smooth muscle cells (VSMC), and adventitial fibroblasts (AF). Following treatment with 1 μM Angiotensin II (Ang II) for 24 hours, TSP2 protein expression is highest in fibroblasts among the major vascular wall cell types examined (Figure 3C). Immunofluorescence staining further confirmed the subcellular location of TSP2 primarily in the cytoplasm (Figure 3D). In three distinct experimental AAA mouse models, TSP2 protein is primarily localized in the aortic adventitia and exhibits significant colocalization with the fibroblast marker ER-TR7 (Figure 3E). This finding confirms that TSP2 is predominantly

expressed in adventitial fibroblasts.

To investigate the effect of Ang II on TSP2 protein expression in fibroblasts, we treated fibroblasts with 1 μM Ang II to simulate the pathological process of AAA. Cell samples were collected at various time points. PCR and Western blot analyses showed that TSP2 mRNA and TSP2 protein expression levels initially increased following Ang II treatment, peaking at around 12 to 24 hours, before subsequently declining (Figures 3F and 3G). A similar pattern was also observed in experiments using 0.4 U/mL porcine pancreatic elastase (PPE) treatment (Figure 3H). [27].

3.4. TSP2 enhances ECM content and strength

To interrogate the biological role of TSP2, we conducted bulk transcriptomic analysis in primary human aortic adventitial fibroblasts with TSP2 knockdown or overexpression. Heatmap analysis identified the 10 most significantly upregulated and downregulated genes in each group (Figure 4A). Gene Ontology (GO) enrichment analysis revealed that differentially expressed genes (DEGs) were associated with collagen-containing extracellular matrix, cell-matrix adhesion, and focal adhesion (Figure 4B). The Molecular Function analysis showed that DEGs were related to glycosaminoglycan binding and integrin binding (Supplementary Figure 4A-4E).

PRELP is an extracellular matrix protein that plays a critical role in stabilizing collagen fibrils and mediating cell-matrix interactions, while TGM2 is a calcium-dependent enzyme involved in cross-linking extracellular matrix proteins and regulating cell signaling pathways. WB and quantitative analysis showed that TSP2 overexpression (OE) increased the levels of key ECM components, including Collagen I, Collagen III, Fibronectin, PRELP (Proline/arginine-rich end leucine-rich repeat protein), and TGM2(Transglutaminase 2) , while TSP2 knockdown (KD) reduced the expression of these proteins (Figure 4C and 4D). IF staining also confirmed that TGM2 and PRELP expression were higher in AAA patients compared to healthy controls (Figure 4E).

Cell adhesion assays revealed that TSP2 overexpression (OE) significantly enhanced, while its knockdown (KD) reduced adhesion capacity in fibroblast (Figure 4F). In contrast, TSP2

alterations elicited minimal impacts on fibroblast proliferation as evidenced in by CCK8 cell proliferation assay (Supplementary Figure 3F). To investigate the effect of TSP2 on fibroblasts' ability to contract the collagen matrix, a collagen gel contraction assay was performed. TSP2 overexpression (OE) demonstrated greater contraction of the collagen matrix, while TSP2 knockdown (KD) exhibited reduced contraction capacity (Figures 4G). Transmission electron microscopy (TEM) revealed that, compared to $TSP2^{+/+}$ mouse, $TSP2^{-/-}$ mice exhibit reduced collagen fiber content, lower density, and disorganized fiber arrangement in the abdominal aortic tissue, with fewer connections between fibroblasts and collagen fibers (Figure 4H).

3.5. TSP2 expression is regulated by the Akt/STAT3 pathway

To elucidate the upstream regulatory mechanism of TSP2, we first profiled the predicted transcription factor binding sites in the promoter region of TSP in JASPAR, with STAT3 as the top ranked candidate (Figure 5A). To validate the cis-transcriptional regulation of STAT3 over TSP2, we introduced a constitutively active form of exogenous STAT3 (P750Y) in mouse adventitial fibroblasts using a lentiviral vector, which led to an increase in TSP2 protein expression. Conversely, inhibiting STAT3 activation (p-STAT3) with AG490 resulted in reduced TSP2 protein expression (Figure 5B).

We further performed chromatin immunoprecipitation (ChIP) with antibodies specific to either total or activated STAT3 in adventitial fibroblasts, followed by PCR to amplify the specific promoter regions of TSP2 as predicted. As shown in Figure 5Cthe TSP2 gene promoter was positively amplified, while no positive amplification occurred with the control IgG antibody.

This confirms that the positive amplification of the TSP2 promoter is specific to STAT3 and p-STAT3. Additionally, we identified the binding sequence of STAT3 to the TSP2 gene promoter.

In pursuit of the machinery governing STAT3 activity, we chose to investigate the role of Akt (protein kinase B), a serine/threonine kinase widely involved in regulating cell growth, survival, and metabolism. Indeed, Akt has previously been reported to enhance STAT3 transcriptional activity by phosphorylating STAT3 at the Ser727 residue [34]. We modulated Akt activity using adenoviral vectors expressing either a myristoylated constitutively active Akt mutant (Ad-Akt-on) or a dominant-negative Akt mutant (Ad-Akt-off). WB and IF showed that enhancing AKT activity led to increased expression of p-STAT3 and TSP2, while inhibition of AKT activity reduced the expression of p-STAT3 and TSP2 (Figure 5D and 5E). Furthermore, overexpression of STAT3 in mouse adventitial fibroblasts with inhibited AKT activity still resulted in increased TSP2 expression (Figure 5F).

3.6.Exogenous TSP2 Delivery Rescues AAA Progression

To confirm that the AAA-susceptible phenotype of $TSP2^{-/-}$ is primarily mediated by its loss-of-function in aorta, especially the adventitia, we conducted a functional rescue experiment to re-introduce TSP2 protein to TSP2 global knockout mice. Briefly, a slow-release hydrogel [30] containing recombinant TSP2 protein was applied locally to the infrarenal abdominal aortic segment immediately following the intraluminal elastase perfusion (Figure 6A). In the control group, $TSP2^{-/-}$ mice were subjected to the same elastase procedure, followed by peri-aortic application with empty hydrogel. Fourteen days post-treatment, the maximum aneurysm

diameter was measured using Doppler ultrasound. The results showed that, compared to the empty hydrogel group (KO), the group receiving exogenous TSP2 protein (rescue) had a lower AAA formation rate and smaller aneurysm diameter (Figures 6B-D). Similarly, H&E, Masson, and VVG staining were performed on tissue sections from both groups of mouse (Figure 6E). Quantification of adventitial thickness show that the control $TSP2^{-/-}$ mice (KO) exhibited significantly reduced adventitial thickness compared to $TSP2^{-/-}$ mice rescued with exogenous TSP2 (rescue) (Figure 6F). Histologically, quantitative analysis of collagen fibers in Masson-stained images revealed that the TSP2-rescued mice contained higher collagen fiber content compared to $TSP2^{-/-}$ mice (KO) (Figure 6G). VVG staining showed fewer elastic fiber ruptures and better-organized fiber arrangement in the TSP2-rescued mice compared to the $TSP2^{-/-}$ mice (KO) (Figure 6H).

3.7. Lentiviral TSP2 Overexpression Attenuates AAA Progression

To further determine the therapeutic potential of local TSP2 restoration, we performed a lentivirus-mediated TSP2 overexpression in wild-type male mice. Briefly, a hydrogel (Pluronic F127) containing lentivirus overexpressing TSP2 was delivered to $TSP2^{+/+}$ mice in the elastase-induced AAA model (Figure 7A). Fourteen days after treatment, Doppler ultrasound analysis showed that, compared to the control group receiving control lentivirus (control), the TSP2 overexpression group (OE) had a lower AAA formation rate and smaller aneurysm diameter (Figures 7B-D) Similarly, H&E, Masson, and VVG staining were performed on tissue sections from both groups of mouse (Figure 7E). The results showed that the TSP2 overexpression group (OE) had thicker adventitia and higher collagen fiber content compared to the control

group (Figure 7F and G). The TSP2 overexpression group (OE) also exhibited fewer elastic fiber ruptures and more organized fiber arrangement (Figure 7H).

Discussion

AAA remains a life-threatening condition with no effective pharmacotherapies or reliable prognostic markers to predict disease progression or rupture risk. In this study, we provide several novel findings that address critical gaps in our understanding of AAA. First, although previous studies have reported upregulated TSP2 expression in the tissues and plasma of AAA patients, this study is the first to use in situ analysis and bioinformatics approaches to identify fibroblasts as the primary cellular source of TSP2 in AAA tissues. Second, our findings from TSP2 loss-of-function and rescue experiments provide the first direct evidence supporting TSP2's protective role in AAA by enhancing ECM integrity and attenuating disease progression. Third, we identify a new upstream regulatory mechanism, demonstrating that TSP2 expression is modulated via the Akt/STAT3 signaling pathway, further elucidating its role in vascular homeostasis. Importantly, unlike prior studies suggesting TSP2 promotes cardiovascular or aortic pathologies [35] [36,37], our data reveal that TSP2 instead acts as a stabilizing factor in AAA, highlighting its unique role in maintaining vascular integrity. These findings underscore TSP2's potential as a therapeutic target for AAA and open new avenues for biomarker and drug development in this unmet medical need.

The structural integrity and function of the aortic wall largely depend on ECM components, particularly the orderly arrangement of collagen fibers [38]. Traditionally, ECM remodeling has

been associated with the progression of vascular diseases such as AAA [39], where abnormal collagen fiber organization reduces vascular mechanical performance [32 40 41]. However, this study highlights the unique role of TSP2 in this process. Unlike typical pathological remodeling, TSP2 enhances ECM synthesis and organization, promoting collagen fiber alignment and increasing the strength of the aneurysm wall, thereby challenging the traditional view that ECM remodeling invariably exacerbates disease progression.

The expression of TSP2 is regulated by multiple signaling pathways, such as PI3K/Akt, NF-κB, and TGF-β/Smad axes. Previous studies have shown that activation of the PI3K/Akt pathway typically suppresses TSP2 expression [42 43], thereby affecting ECM remodeling, whereas NF-κB-mediated inflammatory signaling may promote TSP2 upregulation [19 44]. Additionally, TGF-β can enhance TSP2 transcription via Smad2/3 [45], influencing vascular remodeling. Notably, microRNAs may also regulate TSP2 expression; for example, miR-1228 is known to target TSP2 mRNA for degradation [46 47], thereby affecting ECM metabolism.In this study, we further identified the STAT3/AKT axis as a critical upstream regulatory factor of TSP2. Our experimental results demonstrated that enhancing STAT3 phosphorylation significantly increases TSP2 expression, whereas inhibiting AKT phosphorylation reduces both STAT3 and TSP2 expression. Furthermore, ChIP assays confirmed that STAT3 can directly bind to the TSP2 promoter region and promote its transcription.These findings highlight the critical role of the STAT3/AKT axis in AAA progression and suggest its potential as a therapeutic target. Future studies should further explore its molecular mechanisms and assess the feasibility of targeted interventions.

Currently, there are no recommended pharmacological treatments or therapeutic regimens for small AAA in clinical practice[48]. While statins [49], angiotensin-converting enzyme inhibitors (ACEIs) [50], angiotensin II receptor blockers (ARBs) [51], beta-blockers [52], hypoglycemic agents (such as metformin [53]), and antibiotics (including doxycycline [54] and roxithromycin [55]) have shown efficacy in slowing aneurysm progression in animal models, their effectiveness in humans remains unverified. Developing novel and effective treatments for small AAAs is therefore an urgent priority. Systemic delivery of TSP2 has limited efficacy due to its short half-life and poor targeting[56]. Inspired by localized cardiac drug delivery strategies [57], this study employed TSP2 hydrogel-based localized delivery to enhance its targeting efficiency and biological stability. Our study found that in $TSP2^{-/-}$ mice, administration of exogenous TSP2 protein restored ECM remodeling and stabilized the aneurysm wall, exhibiting a rescue effect. In $TSP2^{+/+}$ mice, TSP2 overexpression enhanced ECM integrity and slowed AAA progression, demonstrating a therapeutic effect. These findings confirm the critical protective role of TSP2 in AAA and support hydrogel-based localized delivery as a potential therapeutic strategy. However, this study employed a preventive model, where TSP2 was administered before AAA formation. However, in clinical practice, treatment should target existing AAA rather than being solely preventive [58]. Therefore, future studies should shift towards a therapeutic model, where TSP2 is administered after aneurysm formation, to better simulate real-world clinical applications.

This study has several limitations that should be considered. First, no single experimental model could fully recapitulate the complex disease process of AAA onset and progression.

While we utilized the elastase-induced AAA model, future studies should incorporate other models, such as Ang II+BAPN or hypercholesterolemia, to better capture the diverse pathological mechanisms underlying AAA. Second, the clinical data in this study were derived from a retrospective rather than a prospective study, making it impossible to predict AAA rupture risk. Additionally, no multivariable analysis was performed to exclude confounding factors, and the sample size may be underpowered, potentially affecting the robustness of our conclusions. Third, sex differences as a biologically relevant variable have not been fully evaluated. This is mainly because AAA exhibits significant sex dimorphism, with a markedly higher incidence in males than in females. Furthermore, this study employed a prevention model rather than a strictly therapeutic study design, meaning TSP2 was administered before AAA formation to assess its preventive effects. Finally, while this study established the role of TSP2 in ECM remodeling, the specific downstream signaling pathways and molecular mechanisms remain unexplored.

In conclusion, our study elucidates the significant role of TSP2 in the progression of AAAs through its influence on extracellular matrix remodeling and vascular stability. Our findings indicate that TSP2 not only aids in the secretion of collagen but also enhances its ordered arrangement, increasing the thickness and strength of the aneurysm wall. Given the lack of effective pharmacological treatments for small AAA, targeting TSP2 presents a promising therapeutic strategy that warrants further exploration in preclinical and clinical settings. Understanding the precise role of TSP2 could pave the way for novel interventions aimed at mitigating the risks associated with AAA progression.

Conclusion

This study reveals that TSP2 is a key endogenous protector maintaining ECM integrity in AAA. TSP2, mainly secreted by adventitial fibroblasts, stabilizes the aortic wall by promoting collagen secretion and organized fiber alignment. Loss of TSP2 leads to ECM disorganization and accelerates aneurysmal expansion, whereas genetic or local restoration of TSP2 reconstructs aortic architecture and suppresses AAA progression. Its transcription is regulated by the Akt/STAT3 signaling pathway, providing a molecular basis for vascular homeostasis. In summary, TSP2 is redefined as a structural "guardian" of the aorta and offers a theoretical and translational basis for localized TSP2 therapy.

Abbreviations:

AAA = Abdominal Aortic Aneurysm

ECM = Extracellular Matrix

TSP2 =Thrombospondin-2

EVAR = Endovascular Aneurysm Repair

AF = Adventitial Fibroblast

Declarations

Funding

This work was supported by the Zhejiang Provincial Natural Science Foundation [KLY26H020025] , the National Natural Science Foundation of China [grant numbers 82470489, 82300472]; and the Zhejiang Provincial Natural Science Foundation [LQ21H020007].

Acknowledgements

We thank Liya Lin and Lihong Chen at Research Center for Life Science and Human Health of Binjang Institute of Zhejiang University, for their help in laboratory management and technical support. We thank Yinping Lyu at the Center of Cryo-Electron Microscopy (CCEM), Zhejiang University, for her technical assistance with transmission electron microscopy. We also acknowledge the sequencing services provided by the LC-Bio platform. The graphical abstract was created using https://BioRender.com.

Authors' contributions

L.H. performed the majority of the experiments, acquired and analyzed the data, and wrote the manuscript. Z.L., L.Y., and H.Z. constructed the mouse models. Y. J. generated the double-gene knockout mice. N.Y. participated in tissue collection and performed ChIP assays, Transwell migration assays, cell contraction, and adhesion experiments. K.Z. and H.M. conducted the bioinformatics analyses. Y.C., J.C., W.Z., L.L., L.C., D.H., and K.C. assisted with animal handling and tissue collection. C.X., M.G., and P.G. reviewed and revised the manuscript. J. Y. and Y.G. provided and organized clinical information related to abdominal aortic aneurysm patients. J.S., L.Z., B.W., and Z.L. designed the study, contributed to data analysis, and co-wrote the manuscript.

Availability of data and material

The datasets generated and/or analyzed during the current study are available from the corresponding author on reasonable request.

Ethics approval and consent to participate

The study complies with the Declaration of Helsinki for the ethical treatment of human specimens and was approved by the Human Research Ethics Committee of the Second Affiliated Hospital, School of Medicine, Zhejiang University (No.2016-085). All animal husbandry and experiments were approved by the Laboratory Animal Ethics Committee of the Second Affiliated Hospital, School of Medicine, Zhejiang University (No. 2022-087).

Competing interest: The authors declare that they have no competing interests.

Consent for publication: All authors have read and approved the final version of the manuscript and consent to its publication in the *Journal of Biomedical Science*.

References

1. Nordon IM, Hinchliffe RJ, Loftus IM, Thompson MM. Pathophysiology and epidemiology of abdominal aortic aneurysms. *Nat Rev Cardiol* 2011; **8**(2): 92-102.

2. Lederle FA, Johnson GR, Wilson SE, et al. The aneurysm detection and management study screening program: validation cohort and final results. Aneurysm Detection and Management Veterans Affairs Cooperative Study Investigators. *Arch Intern Med* 2000; **160**(10): 1425-30.

3. Vardulaki KA, Walker NM, Day NE, Duffy SW, Ashton HA, Scott RA. Quantifying the risks of hypertension, age, sex and smoking in patients with abdominal aortic aneurysm. *Br J Surg* 2000; **87**(2): 195-200.

4. Singh K, Bønaa KH, Jacobsen BK, Bjørk L, Solberg S. Prevalence of and risk factors for abdominal aortic aneurysms in a population-based study : The Tromsø Study. *Am J Epidemiol* 2001; **154**(3): 236-44.

5. Soares Ferreira R, Gomes Oliveira N, Oliveira-Pinto J, et al. Review on management and outcomes of ruptured abdominal aortic aneurysm in women. *J Cardiovasc Surg (Torino)* 2018; **59**(2): 195-200.

6. Powell JT, Brady AR, Brown LC, et al. Long-term outcomes of immediate repair compared

with surveillance of small abdominal aortic aneurysms. *N Engl J Med* 2002; **346**(19): 1445-52.

7. Baman JR, Eskandari MK. What Is an Abdominal Aortic Aneurysm? *Jama* 2022; **328**(22): 2280.

8. Mortality results for randomised controlled trial of early elective surgery or ultrasonographic surveillance for small abdominal aortic aneurysms. The UK Small Aneurysm Trial Participants. *Lancet* 1998; **352**(9141): 1649-55.

9. Wu J, Wang W, Chen Z, Xu F, Zheng Y. Proteomics applications in biomarker discovery and pathogenesis for abdominal aortic aneurysm. *Expert Rev Proteomics* 2021; **18**(4): 305-14.

10. Sakalihasan N, Limet R, Defawe OD. Abdominal aortic aneurysm. *Lancet* 2005; **365**(9470): 1577-89.

11. Limet R, Sakalihassan N, Albert A. Determination of the expansion rate and incidence of rupture of abdominal aortic aneurysms. *J Vasc Surg* 1991; **14**(4): 540-8.

12. Glimåker H, Holmberg L, Elvin A, et al. Natural history of patients with abdominal aortic aneurysm. *Eur J Vasc Surg* 1991; **5**(2): 125-30.

13. Didangelos A, Yin X, Mandal K, et al. Extracellular matrix composition and remodeling in human abdominal aortic aneurysms: a proteomics approach. *Mol Cell Proteomics* 2011; **10**(8): M111.008128.

14. Jones B, Tonniges JR, Debski A, et al. Collagen fibril abnormalities in human and mice abdominal aortic aneurysm. *Acta Biomater* 2020; **110**: 129-40.

15. Adams JC, Lawler J. The thrombospondins. *Cold Spring Harb Perspect Biol* 2011; **3**(10): a009712.

16. Plana E, Oto J, Medina P, et al. Thrombospondins in human aortic aneurysms. *IUBMB Life*

2022; **74**(10): 982-94.

17. Liu Z, Morgan S, Ren J, et al. Thrombospondin-1 (TSP1) contributes to the development of vascular inflammation by regulating monocytic cell motility in mouse models of abdominal aortic aneurysm. *Circ Res* 2015; **117**(2): 129-41.

18. Lee R, Charles PD, Lapolla P, et al. Integrated Physiological and Biochemical Assessments for the Prediction of Growth of Abdominal Aortic Aneurysms in Humans. *Ann Surg* 2019; **270**(1): e1-e3.

19. Pohjolainen V, Mustonen E, Taskinen P, et al. Increased thrombospondin-2 in human fibrosclerotic and stenotic aortic valves. *Atherosclerosis* 2012; **220**(1): 66-71.

20. Topol EJ, McCarthy J, Gabriel S, et al. Single nucleotide polymorphisms in multiple novel thrombospondin genes may be associated with familial premature myocardial infarction. *Circulation* 2001; **104**(22): 2641-4.

21. Plana E, Gálvez L, Medina P, et al. Identification of Novel microRNA Profiles Dysregulated in Plasma and Tissue of Abdominal Aortic Aneurysm Patients. *Int J Mol Sci* 2020; **21**(13).

22. Charan J, Kantharia ND. How to calculate sample size in animal studies? *J Pharmacol Pharmacother* 2013; **4**(4): 303-6.

23. Liu Z, Wang Q, Ren J, et al. Murine abdominal aortic aneurysm model by orthotopic allograft transplantation of elastase-treated abdominal aorta. *J Vasc Surg* 2015; **62**(6): 1607-14.e2.

24. Trachet B, Fraga-Silva RA, Jacquet PA, Stergiopulos N, Segers P. Incidence, severity, mortality, and confounding factors for dissecting AAA detection in angiotensin II-infused mice:

a meta-analysis. *Cardiovasc Res* 2015; **108**(1): 159-70.

25. Yamanouchi D, Morgan S, Stair C, et al. Accelerated aneurysmal dilation associated with apoptosis and inflammation in a newly developed calcium phosphate rodent abdominal aortic aneurysm model. *J Vasc Surg* 2012; **56**(2): 455-61.

26. Jia L, Wang Y, Wang Y, et al. Heme Oxygenase-1 in Macrophages Drives Septic Cardiac Dysfunction via Suppressing Lysosomal Degradation of Inducible Nitric Oxide Synthase. *Circ Res* 2018; **122**(11): 1532-44.

27. Sharma AK, Lu G, Jester A, et al. Experimental abdominal aortic aneurysm formation is mediated by IL-17 and attenuated by mesenchymal stem cell treatment. *Circulation* 2012; **126**(11 Suppl 1): S38-45.

28. Wang G, Yu Y, Sun C, et al. STAT3 selectively interacts with Smad3 to antagonize TGF-β signalling. *Oncogene* 2016; **35**(33): 4388-98.

29. Xu J, Gao M, Fan S, et al. Effect of Akt inhibition on scatter factor-regulated gene expression in DU-145 human prostate cancer cells. *Oncogene* 2007; **26**(20): 2925-38.

30. Chen L, Zhong M, Chen J, et al. Preparation of silk fibroin/hyaluronic acid composite hydrogel based on thiol-ene click chemistry. *Zhejiang Da Xue Xue Bao Yi Xue Ban* 2023; **52**(3): 285-95.

31. Reeps C, Kehl S, Tanios F, et al. Biomechanics and gene expression in abdominal aortic aneurysm. *J Vasc Surg* 2014; **60**(6): 1640-7.e1-2.

32. Fu Y, Zhou Y, Wang K, Li Z, Kong W. Extracellular Matrix Interactome in Modulating Vascular Homeostasis and Remodeling. *Circ Res* 2024; **134**(7): 931-49.

33. Johansson S, Svineng G, Wennerberg K, Armulik A, Lohikangas L. Fibronectin-integrin

interactions. *Front Biosci* 1997; **2**: d126-46.

34. Murase S, McKay RD. Neuronal activity-dependent STAT3 localization to nucleus is dependent on Tyr-705 and Ser-727 phosphorylation in rat hippocampal neurons. *Eur J Neurosci* 2014; **39**(4): 557-65.

35. Oguri M, Kato K, Yokoi K, et al. Association of polymorphisms of THBS2 and HSPA8 with hypertension in Japanese individuals with chronic kidney disease. *Mol Med Rep* 2009; **2**(2): 205-11.

36. Kato K, Oguri M, Kato N, et al. Assessment of genetic risk factors for thoracic aortic aneurysm in hypertensive patients. *Am J Hypertens* 2008; **21**(9): 1023-7.

37. Qi L, Wu K, Shi S, Ji Q, Miao H, Bin Q. Thrombospondin-2 is upregulated in patients with aortic dissection and enhances angiotensin II-induced smooth muscle cell apoptosis. *Exp Ther Med* 2020; **20**(6): 150.

38. Tanios F, Gee MW, Pelisek J, et al. Interaction of biomechanics with extracellular matrix components in abdominal aortic aneurysm wall. *Eur J Vasc Endovasc Surg* 2015; **50**(2): 167-74.

39. Yu ZP, Wang YK, Wang XY, et al. Smooth-Muscle-Cell-Specific Deletion of CD38 Protects Mice from AngII-Induced Abdominal Aortic Aneurysm through Inhibiting Vascular Remodeling. *Int J Mol Sci* 2024; **25**(8).

40. Yanagisawa H, Yokoyama U. Extracellular matrix-mediated remodeling and mechanotransduction in large vessels during development and disease. *Cell Signal* 2021; **86**: 110104.

41. Gasser TC, Gallinetti S, Xing X, Forsell C, Swedenborg J, Roy J. Spatial orientation of

collagen fibers in the abdominal aortic aneurysm's wall and its relation to wall mechanics. *Acta Biomater* 2012; **8**(8): 3091-103.

42. Liu QH, Ma LS. Knockdown of thrombospondin 2 inhibits metastasis through modulation of PI3K signaling pathway in uveal melanoma cell line M23. *Eur Rev Med Pharmacol Sci* 2018; **22**(19): 6230-8.

43. Deng B, Liu XP, Wang X. Prognostic and Immunological Role of THBS2 in Colorectal cancer. *Biomed Res Int* 2021; **2021**: 1124985.

44. Yu C, Wu D, Zhao C, Wu C. Overexpressed Thrombospondin 2 Induced Osteogenic Differentiation of Valve Interstitial Cells via Inhibition of Akt/NF-κB Signaling Pathway to Promote Calcific Aortic Valve Disease Development. *Dis Markers* 2022; **2022**: 2022958.

45. Kimura T, Iwadare T, Wakabayashi SI, et al. Thrombospondin 2 is a key determinant of fibrogenesis in non-alcoholic fatty liver disease. *Liver Int* 2024; **44**(2): 483-96.

46. Mo T, Fu Q, Hu X, Fu Y, Li J. MicroRNA 1228 Mediates the Viability of High Glucose-Cultured Renal Tubule Cells through Targeting Thrombospondin 2 and PI3K/AKT Signaling Pathway. *Kidney Blood Press Res* 2022; **47**(1): 1-12.

47. Lindert S, Wickert L, Sawitza I, et al. Transdifferentiation-dependent expression of alpha-SMA in hepatic stellate cells does not involve TGF-beta pathways leading to coinduction of collagen type I and thrombospondin-2. *Matrix Biol* 2005; **24**(3): 198-207.

48. Chen J, Hu L, Liu Z. Medical treatments for abdominal aortic aneurysm: an overview of clinical trials. *Expert Opin Investig Drugs* 2024; **33**(9): 979-92.

49. Schouten O, van Laanen JH, Boersma E, et al. Statins are associated with a reduced infrarenal abdominal aortic aneurysm growth. *Eur J Vasc Endovasc Surg* 2006; **32**(1): 21-6.

50. Sweeting MJ, Thompson SG, Brown LC, Greenhalgh RM, Powell JT. Use of angiotensin converting enzyme inhibitors is associated with increased growth rate of abdominal aortic aneurysms. *J Vasc Surg* 2010; **52**(1): 1-4.

51. Kristensen KE, Torp-Pedersen C, Gislason GH, Egfjord M, Rasmussen HB, Hansen PR. Angiotensin-converting enzyme inhibitors and angiotensin II receptor blockers in patients with abdominal aortic aneurysms: nation-wide cohort study. *Arterioscler Thromb Vasc Biol* 2015; **35**(3): 733-40.

52. Propranolol for small abdominal aortic aneurysms: results of a randomized trial. *J Vasc Surg* 2002; **35**(1): 72-9.

53. Fujimura N, Xiong J, Kettler EB, et al. Metformin treatment status and abdominal aortic aneurysm disease progression. *J Vasc Surg* 2016; **64**(1): 46-54.e8.

54. Baxter BT, Pearce WH, Waltke EA, et al. Prolonged administration of doxycycline in patients with small asymptomatic abdominal aortic aneurysms: report of a prospective (Phase II) multicenter study. *J Vasc Surg* 2002; **36**(1): 1-12.

55. Vammen S, Lindholt JS, Ostergaard L, Fasting H, Henneberg EW. Randomized double-blind controlled trial of roxithromycin for prevention of abdominal aortic aneurysm expansion. *Br J Surg* 2001; **88**(8): 1066-72.

56. Bein K, Ware JA, Simons M. Myb-dependent regulation of thrombospondin 2 expression. Role of mRNA stability. *J Biol Chem* 1998; **273**(33): 21423-9.

57. Johnson TD, Christman KL. Injectable hydrogel therapies and their delivery strategies for treating myocardial infarction. *Expert Opin Drug Deliv* 2013; **10**(1): 59-72.

58. Lu HS, Owens AP, 3rd, Liu B, Daugherty A. Illuminating the Importance of Studying

1 Interventions on the Propagation Phase of Experimental Mouse Abdominal Aortic Aneurysms.

2 *Arterioscler Thromb Vasc Biol* 2021; **41**(4): 1518-20.

3

Figures:

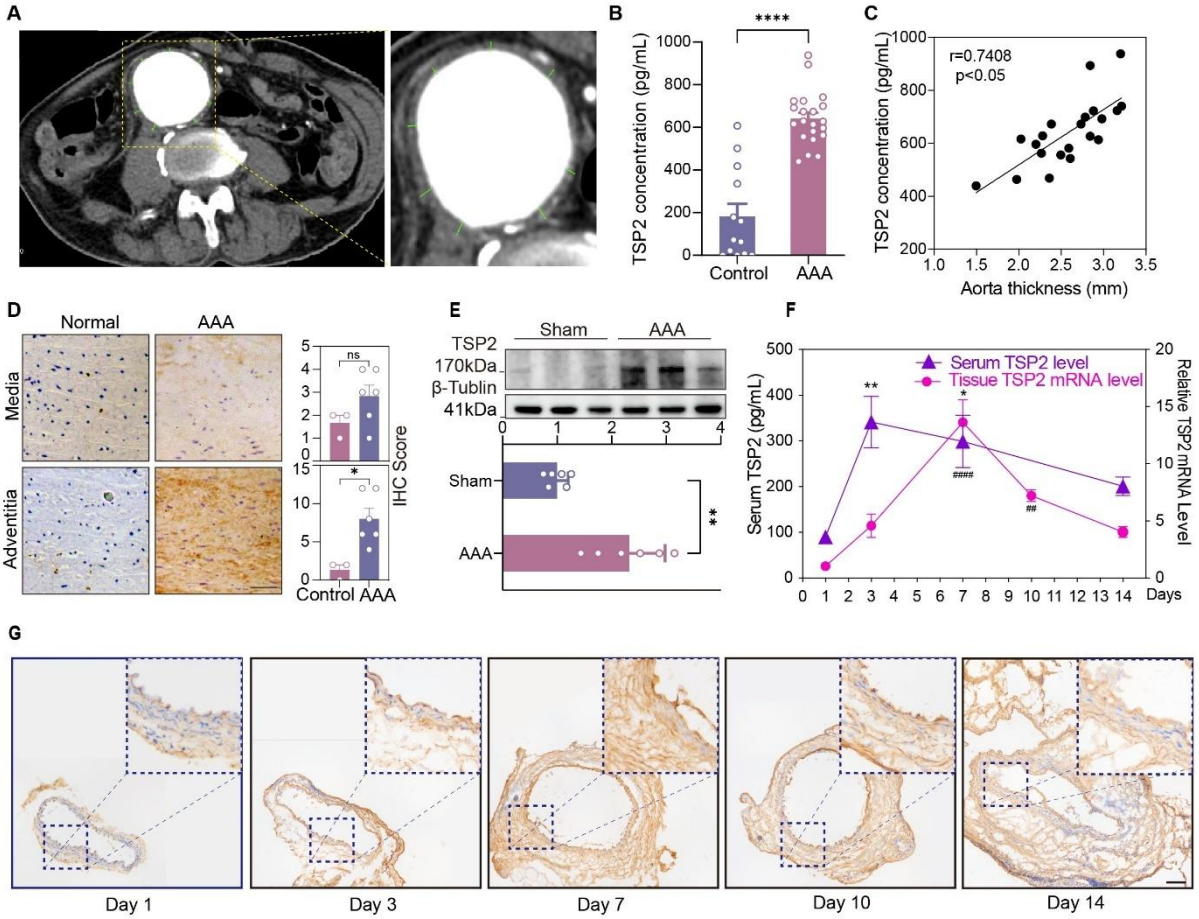

Figure 1: TSP2 predominantly localizes to the adventitia and exhibits dynamic temporal changes in AAA.

(A)Representative CT imaging of AAA. The thickness of the aneurysm wall was evaluated from eight different directions (indicated by green lines). (B) Enzyme-Linked Immunosorbent Assay (ELISA) analysis of serum TSP2 levels in healthy controls (n=13) and AAA patients (n=21). TSP2 levels were significantly elevated in AAA patients compared to healthy controls. (C) Correlation between serum TSP2 concentration and aortic wall thickness in AAA patients (n=21). A significant positive correlation was observed ($r = 0.7408$, $p < 0.05$). (D) IHC staining of TSP2 in the aortic wall of healthy controls (n=3) and AAA patients (n=6). TSP2 was

moderately increased in the media and substantially elevated in the adventitia of AAA tissues. Right panel shows IHC scores, indicating significant differences in TSP2 expression in the adventitia. Scale bars = 20μm. (E) WB analysis of tissue TSP2 protein levels in sham-operated (n=7) and elastase perfusion-induced AAA mouse models (n=7). TSP2 levels were significantly higher in the AAA group. The lower panel shows quantification of band intensity. (F) Serum TSP2 levels (n=3) and tissue relative TSP2 mRNA levels (n=3) in elastase perfusion-induced AAA mouse models over a 14-day period post-surgery. Serum TSP2 levels peaked at day 3 and subsequently declined, while TSP2 mRNA levels followed a similar trend. Scale bar = 100 μm. (G) IHC staining of TSP2 in elastase perfusion-induced murine AAA tissue sections at different time points (Day 1, 3, 7, 10, and 14). The expression of TSP2 in AAA tissue increased in the early phase and gradually declined. Scale bar = 100 μm. Data are presented as mean ± SEM. Statistical significance was determined by Mann-Whitney U test (B, D and E), Pearson correlation analysis (C) or ordinary one-way analysis of variance (ANOVA) with Dunnett's multiple comparisons correction (F).*P < 0.05, **P <0.01, ***P < 0.001, ****p < 0.0001, ns= not significant, $^{\#}p < 0.05$.

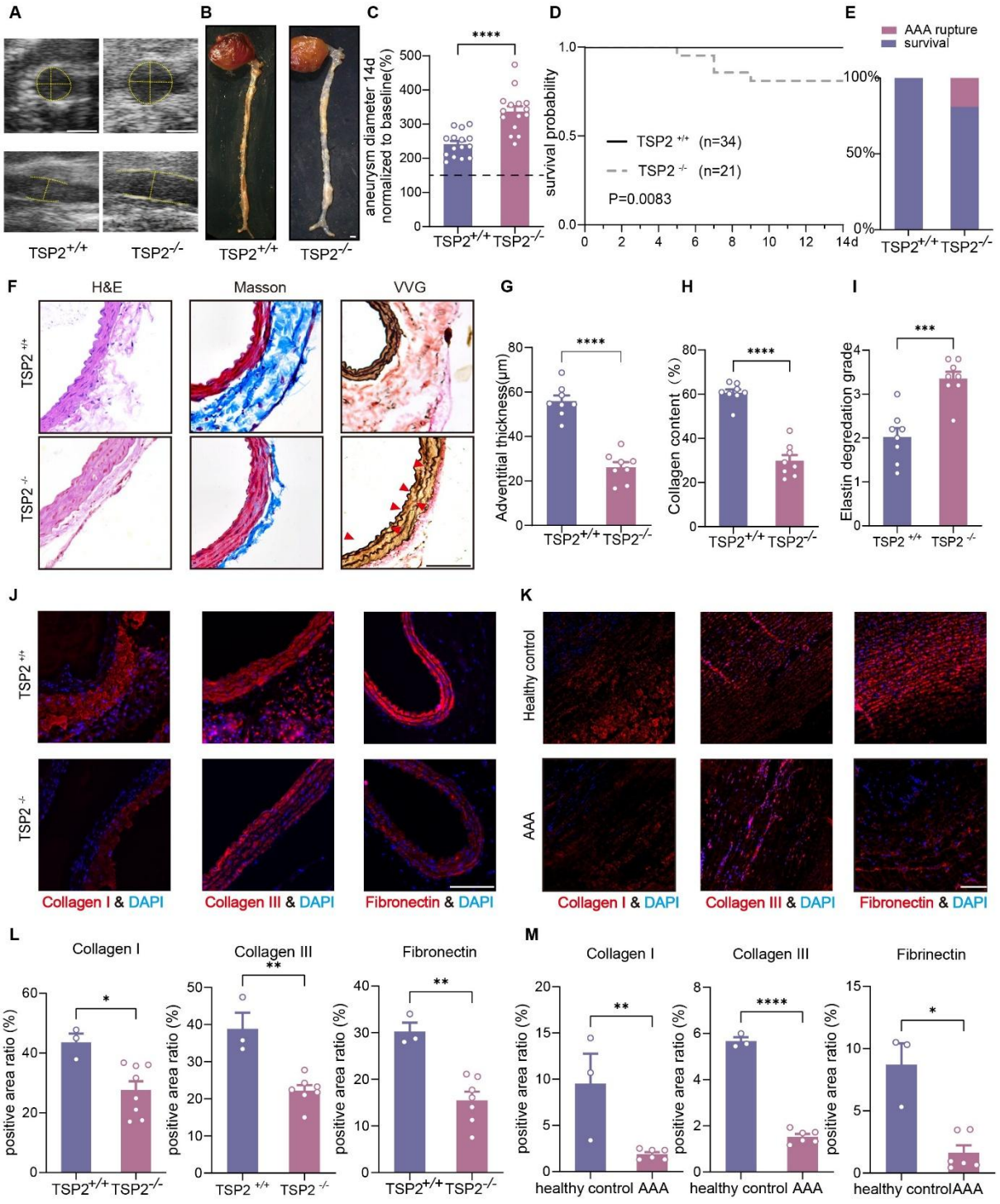

Figure 2: TSP2 deficiency exacerbates ECM degradation and AAA progression.

(A) Representative ultrasound images showing aneurysm formation in $TSP2^{+/+}$ and $TSP2^{-/-}$ mice 14 days after elastase perfusion. Yellow lines indicate the aneurysm diameters. Scale bars = 1mm. (B) Gross appearance of the isolated aortas from $TSP2^{+/+}$ and $TSP2^{-/-}$ mice 14 days

post-perfusion. Yellow arrows indicate enlarged aneurysmal sections in $TSP2^{+/+}$ and $TSP2^{-/-}$ mice. Scale bars = 1mm. (C) Quantification of aneurysm diameter, normalized to baseline, measured 14 days after elastase perfusion in $TSP2^{+/+}$ and $TSP2^{-/-}$ mice. Aneurysm diameter in $TSP2^{-/-}$- mice was significantly larger.(D) Kaplan-Meier survival curve of $TSP2^{+/+}$ (n=34) and $TSP2^{-/-}$ (n=21) mice following elastase perfusion, showing reduced survival probability in $TSP2^{-/-}$ mice (P = 0.0083).(E) In the elastase perfusion-induced AAA model, all $TSP2^{+/+}$ mice (n=34) survived the 14-day observation period, whereas $TSP2^{-/-}$ mice (n=21) exhibited mortality cases, with all four deaths confirmed by necropsy to be caused by aortic rupture (as evidenced by periaortic hematoma formation). (F) Representative histological staining of aortic tissue from $TSP2^{+/+}$ and $TSP2^{-/-}$ mice, including hematoxylin and eosin (H&E), Masson's trichrome, and Verhoeff-Van Gieson (VVG) staining. Red arrowheads in VVG staining indicate fragmented elastic fibers. Scale bars = 100μm. (G) Quantification of adventitial thickness from H&E staining. $TSP2^{-/-}$ mice exhibited significantly reduced adventitial thickness compared to $TSP2^{+/+}$ mice. (H) Collagen content quantified from Masson's trichrome staining. Collagen content was significantly reduced in $TSP2^{-/-}$ mice compared to $TSP2^{+/+}$ mice. (I) Elastin degradation score derived from VVG stained sections. $TSP2^{-/-}$ mice exhibited increased elastin degradation compared to $TSP2^{+/+}$ mice. (J) IF staining of Collagen I, Collagen III, and Fibronectin in aortic tissues from $TSP2^{+/+}$ and $TSP2^{-/-}$ mice. Collagen and fibronectin signals were weaker in $TSP2^{-/-}$ mice compared to $TSP2^{+/+}$ mice. Scale bars = 100μm. (K) IF staining of Collagen I, Collagen III, and Fibronectin in aortic tissues from healthy controls and AAA patients. ECM component levels were reduced in AAA patients compared to healthy controls. Scale bars = 100 μm. (L) Quantitative comparative analysis of immunofluorescence-positive

areas for collagen I, collagen III, and fibronectin in aortic tissues between $TSP2^{-/-}$ and $TSP2^{+/+}$ mice. (M) Quantitative comparative analysis of immunofluorescence-positive areas for collagen I, collagen III, and fibronectin in aortic tissues between healthy controls and AAA patients. Data are shown as mean ± SEM. Statistical significance was determined by unpaired Student's t-test (C, G, H, L and M-Collagen I ,Collagen III), Mantel–Cox test (D), or Mann-Whitney U test (I and M-Fibronectin). *P < 0.05, **P <0.01, ***P < 0.001, ****p < 0.0001, ns= not significant.

Figure 3: Adventitial fibroblasts are the primary source of TSP2 in AAA.

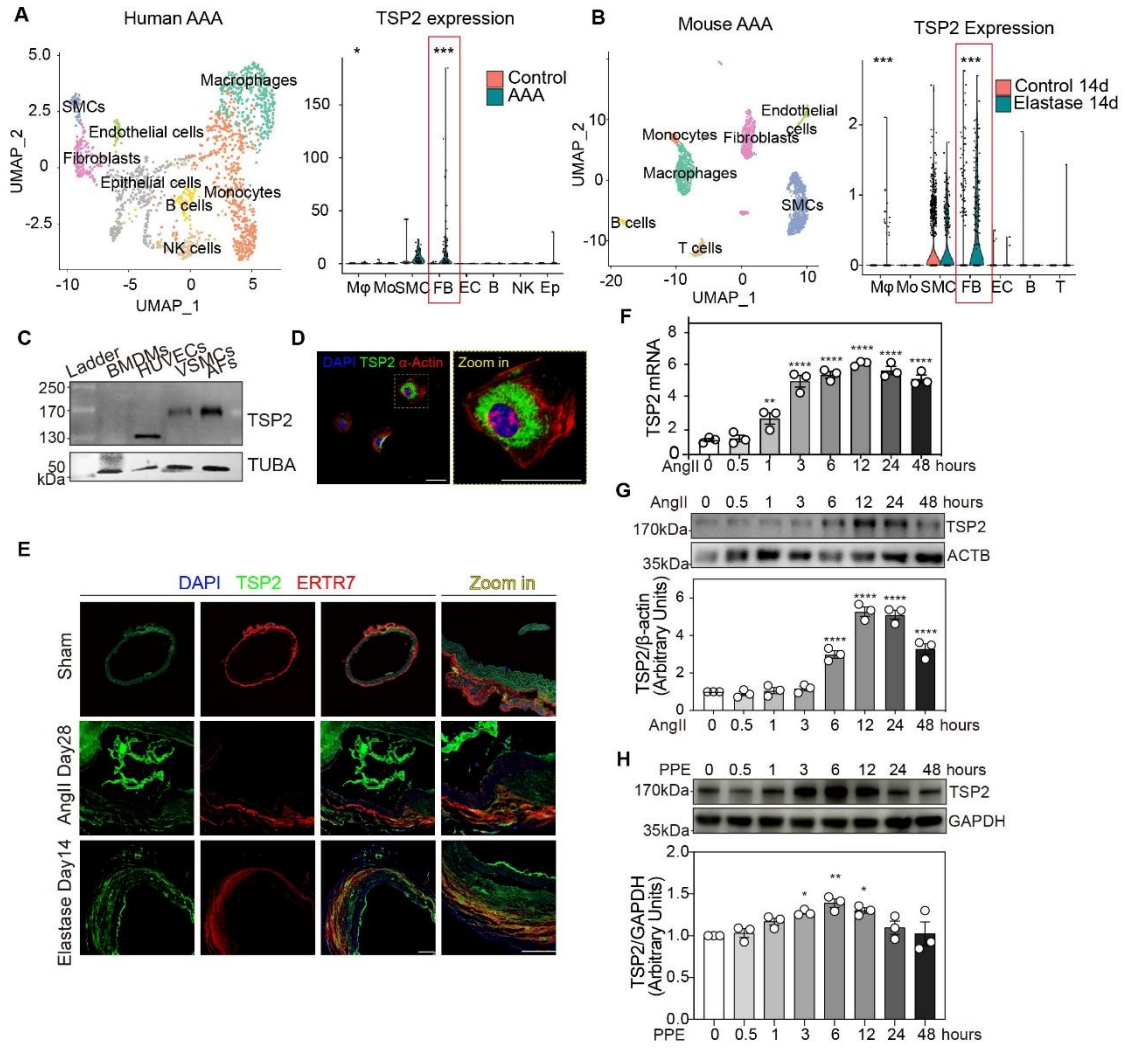

(A)UMAP analysis of human AAA single-cell RNA sequencing data showing clustering of various cell types, including smooth muscle cells (SMC), endothelial cells (EC), fibroblasts (FB), and immune cells. TSP2 expression was predominantly observed in fibroblasts (FB) in AAA compared to control tissues. (B) UMAP analysis of murine AAA model single-cell RNA sequencing data showing distinct cell clusters. TSP2 expression was predominantly detected in fibroblasts (FB) in AAA tissues compared to control. (C) Western blot analysis of TSP2 protein levels in different vascular cell types after treatment with 1 μM Ang II for 24 hours, including bone marrow-derived macrophages (BMDMs), human umbilical vein endothelial

cells (HUVECs) , vascular smooth muscle cells (VSMCs), and adventitial fibroblasts (AFs). TSP2 was predominantly expressed in fibroblasts. (D) IF staining shows colocalization of TSP2 (green) with α-Actin (red) in cultured fibroblasts, indicating high expression of TSP2 in fibroblasts. The zoom-in image shows that TSP2 is primarily localized in the cytoplasm. Scale bars = 20μm. (E) IF staining of aortic tissues from sham-operated mouse, Ang II-induced AAA mouse models and elastase-perfusion-induced AAA mouse models. TSP2 (green) colocalized with the fibroblast marker ERTR7 (red) in the aortic adventitia, indicating fibroblasts as the primary source of TSP2 in AAA. Scale bars = 50μm. (F) RT-qPCR analysis of TSP2 mRNA expression levels in fibroblasts treated with AngII at different time points (n=3). TSP2 mRNA levels significantly increased between 3 to 24 hours. (G) Western blot analysis of TSP2 protein levels in fibroblasts treated with Ang II at different time points (n=3). Quantification of band intensity shows a significant increase in TSP2 protein between 6 to 24 hours. (H) Western blot analysis of TSP2 protein expression in fibroblasts at different time points following PPE treatment. PPE treatment induced a time-dependent increase in TSP2 expression, peaking at 3-12 hours. Data are shown as mean ± SEM. Statistical significance was determined by ordinary one-way analysis of variance (ANOVA) with Dunnett's multiple comparisons correction (F, G and H). *P < 0.05, **P <0.01, ***P < 0.001, ****p < 0.0001, ns= not significant.

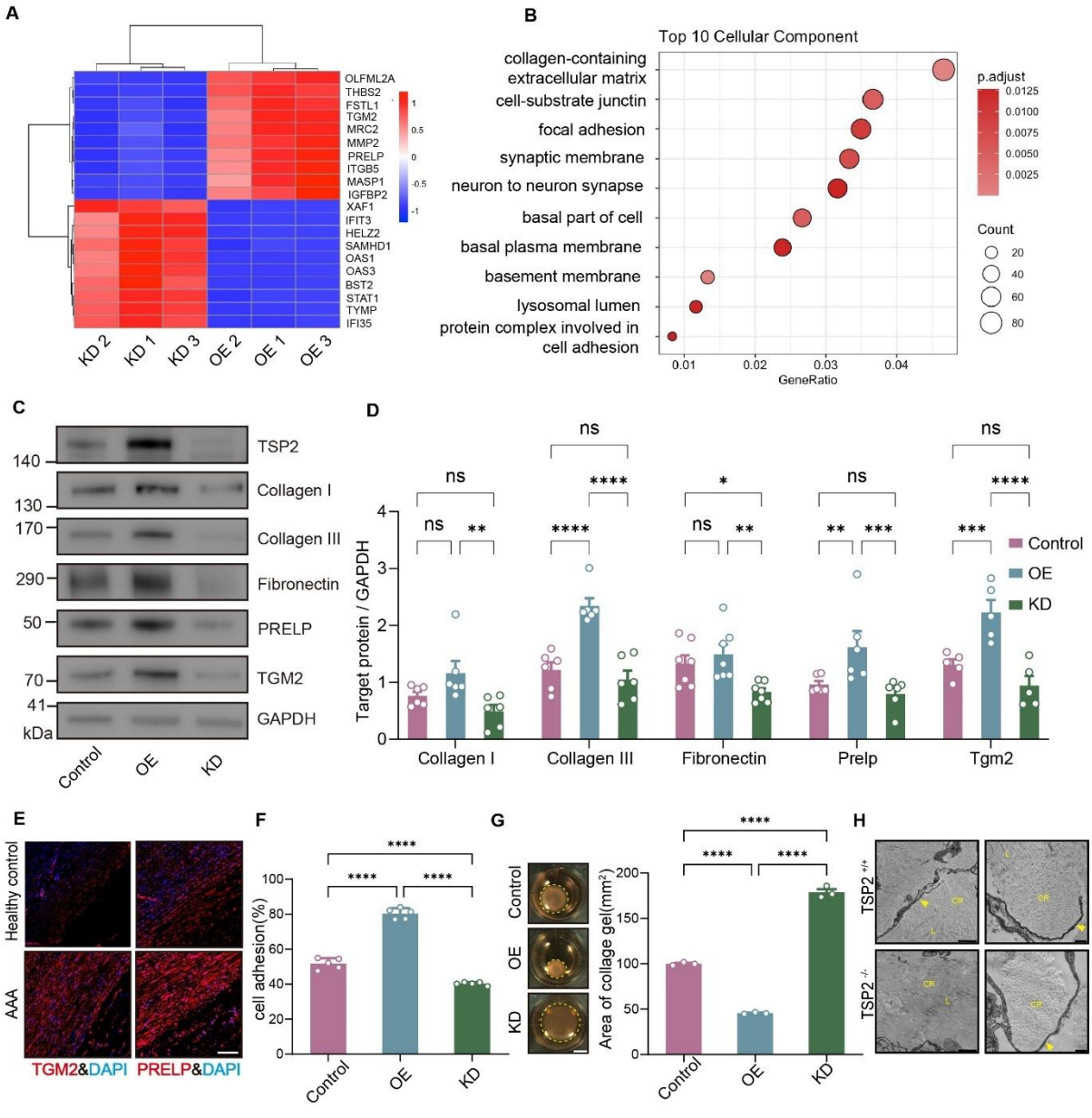

Figure 4: TSP2 promotes ECM content and fibroblast-mediated collagen matrix remodeling. (A) Heatmap showing the top 10 most significantly upregulated and downregulated genes in fibroblasts treated with AngII, comparing the TSP2 overexpression (OE) to the TSP2 knockdown (KD) (n=3). (B) GO Cellular Component analysis of DEGs in fibroblasts treated with Ang II, comparing the TSP2 overexpression (OE) and TSP2 knockdown (KD). Enriched pathways include collagen-containing extracellular matrix and cell-matrix adhesion. (C) Western blot analysis of TSP2, Collagen I, Collagen III, Fibronectin, PRELP, and TGM2

protein levels in fibroblasts treated with Ang II. The expression of these ECM components was elevated in TSP2 overexpression (OE) fibroblasts and reduced in TSP2 knockdown (KD) fibroblasts. (D) Quantification of Western blot analysis for Collagen I, Collagen III, Fibronectin, PRELP, and TGM2 relative to GAPDH in fibroblasts treated with Ang II (n=5~8). (E) IF staining of TGM2 and PRELP in aortic tissues from healthy controls and AAA patients. TGM2 and PRELP levels were higher in AAA tissues compared to healthy aorta. Scale bars = 100μm. (F) Cell adhesion assay showing increased adhesion ability of TSP2 overexpression (OE) fibroblasts and decreased adhesion in TSP2 knockdown (KD) fibroblasts, indicating the role of TSP2 in promoting cell adhesion (n=5). (G**)** Representative images of the collagen gel contraction assay and quantitative analysis of gel area demonstrated that TSP2 overexpressing (OE) fibroblasts treated with Ang II exhibited enhanced collagen gel contraction, whereas TSP2 knockdown (KD) fibroblasts treated with Ang II showed reduced contractility (n=3). Scale bar = 5 mm. (H) TEM images of the abdominal aorta from $TSP2^{+/+}$ and $TSP2^{-/-}$ mice. $TSP2^{-/-}$ mice exhibited disorganized collagen fiber arrangements and reduced density compared to $TSP2^{+/+}$ mice. CR: cross-section; L: longitudinal section; arrows indicate fibroblast-collagen connections. Left column Scale bars = 2 μm, Right column Scale bars = 500 nm. Data are shown as mean ± SEM. Statistical significance was determined by ordinary two-way analysis of variance (ANOVA) with Tukey's multiple comparisons correction (D), or ordinary one-way analysis of variance (ANOVA) with Tukey's multiple comparisons correction (F and G). *P < 0.05, **P <0.01, ***P < 0.001, ****p < 0.0001, ns= not significant.

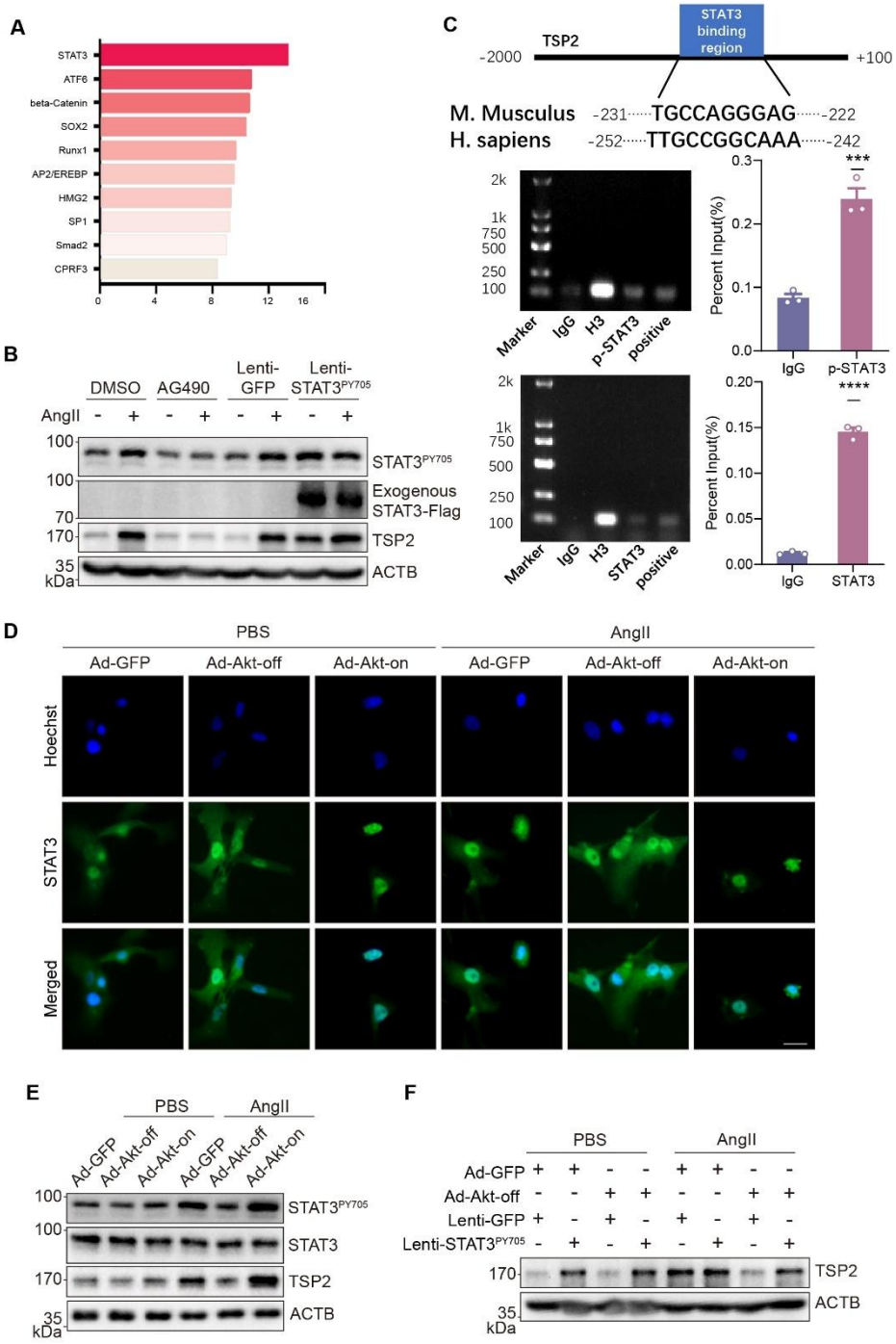

1

2 **Figure 5:** TSP2 expression is regulated by the Akt/STAT3 pathway.

3 (A)Prediction of transcription factors potentially regulating TSP2 using the JASPAR

database.STAT3 is highlighted as the top predicted transcription factor for TSP2 regulation. (B) Western blot analysis showing the effect of STAT3 phosphorylation on TSP2 expression in fibroblasts treated with Ang II. Inhibition of STAT3 phosphorylation with AG490 reduced TSP2 levels, whereas overexpression of STAT3 ($STAT3^{pY705}$) increased TSP2 expression. (C) Schematic representation of the STAT3 binding region in the TSP2 promoter for both mouse and human. Chromatin immunoprecipitation (ChIP) assays using antibodies against STAT3 and phosphorylated STAT3 (p-STAT3) demonstrated their binding to the TSP2 promoter. Positive amplification is shown in ChIP-qPCR results, confirming STAT3 binding (n=3). (D) IF staining of STAT3 (green) and nuclei (Hoechst, blue) in fibroblasts treated with Ad-GFP, Ad-Akt-off, or Ad-Akt-on, either with PBS or Ang II. Results indicate that activation of Akt (Ad-Akt-on) promotes STAT3 nuclear localization in response to Ang II. Scale bars = 20 μm. (E) Western blot analysis of STAT3 and TSP2 expression in fibroblasts transduced with Ad-GFP, Ad-Akt-off, or Ad-Akt-on, in the presence or absence of Ang II. Activation of Akt led to increased STAT3 phosphorylation and TSP2 expression. (F) Western blot analysis of TSP2 expression in fibroblasts under Akt inhibition (Ad-Akt-off), with or without overexpression of STAT3. Overexpression of STAT3 ($STAT3^{pY705}$) restored TSP2 expression despite Akt inhibition, confirming that STAT3 functions downstream of Akt. Data are shown as mean ± SEM. Statistical significance was determined by unpaired Student's t-test (C). *P < 0.05, **P <0.01, ***P < 0.001, ****p < 0.0001, ns= not significant.

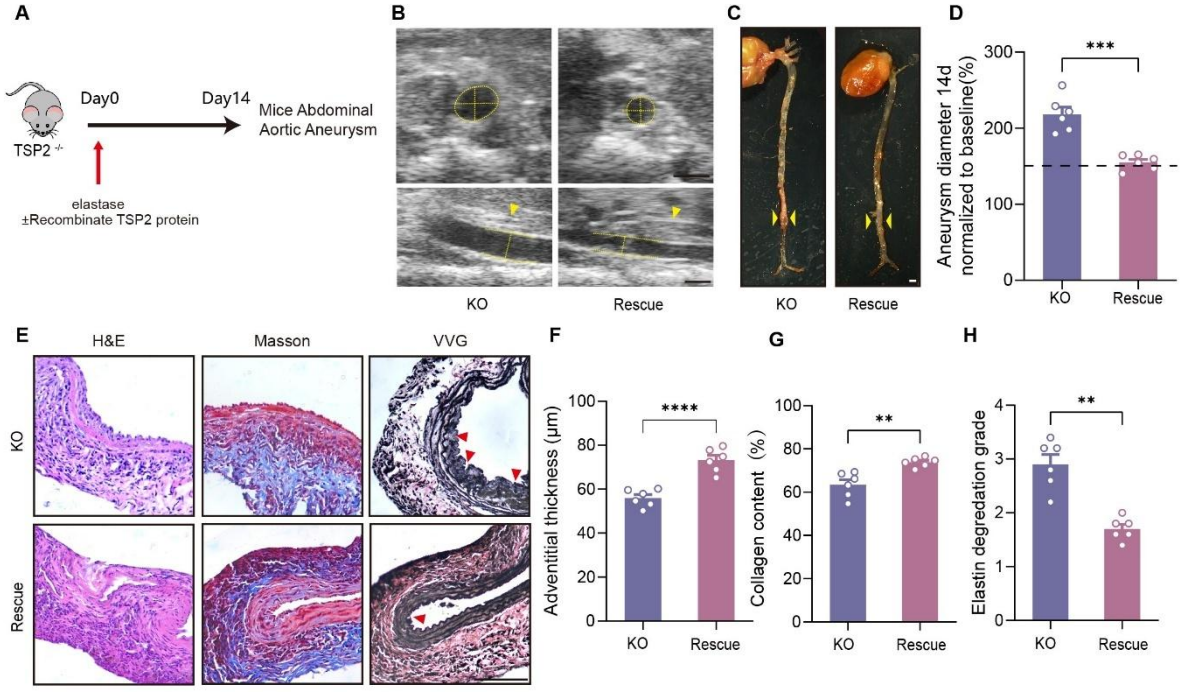

Figure 6: Exogenous TSP2 Delivery Rescue AAA Progression in TSP2 Knockout Mice. Schematic representation of the experimental design. TSP2$^{-/-}$ mice were perfused with elastase on Day 0, with (Rescue) or without (KO) recombinant TSP2 protein. Aortic aneurysm analysis was performed 14 days later. (B) Representative ultrasound images of the abdominal aorta of TSP2$^{-/-}$ mouse treated with (Rescue) or without (KO) TSP2. Yellow dashed lines indicate aneurysm diameter, and arrowheads point to the hydrogel. Scale bars = 1mm. (C) Gross appearance of the isolated aortas from TSP2$^{-/-}$ mice treated with (Rescue) or without (KO) TSP2 14 days post-perfusion. Yellow arrowheads indicate aneurysm. Scale bars = 1 mm. (D) Quantification of aneurysm diameter normalized to baseline measurements, demonstrating a significant reduction in aneurysm size in TSP2$^{-/-}$ mice treated with TSP2 (Rescue) compared to untreated controls (KO) (n=4). (E) Histological staining of aortic sections from TSP2$^{-/-}$ mice treated with (Rescue) or without (KO) TSP2, including H&E, Masson's trichrome, and VVG staining. Red arrowheads in VVG staining indicate

fragmented elastic fibers. Scale bars = 100μm. (F) Quantification of adventitial thickness from H&E staining. TSP2$^{-/-}$ (KO) mice exhibited significantly reduced adventitial thickness compared to TSP2$^{-/-}$ mice treated with TSP2 (Rescue). Data are shown as mean ± SEM. Statistical significance was determined by unpaired Student's t-test (D, F and G), or Mann-Whitney U test (H). *P < 0.05, **P <0.01, ***P < 0.001, ****p < 0.0001, ns= not significant.

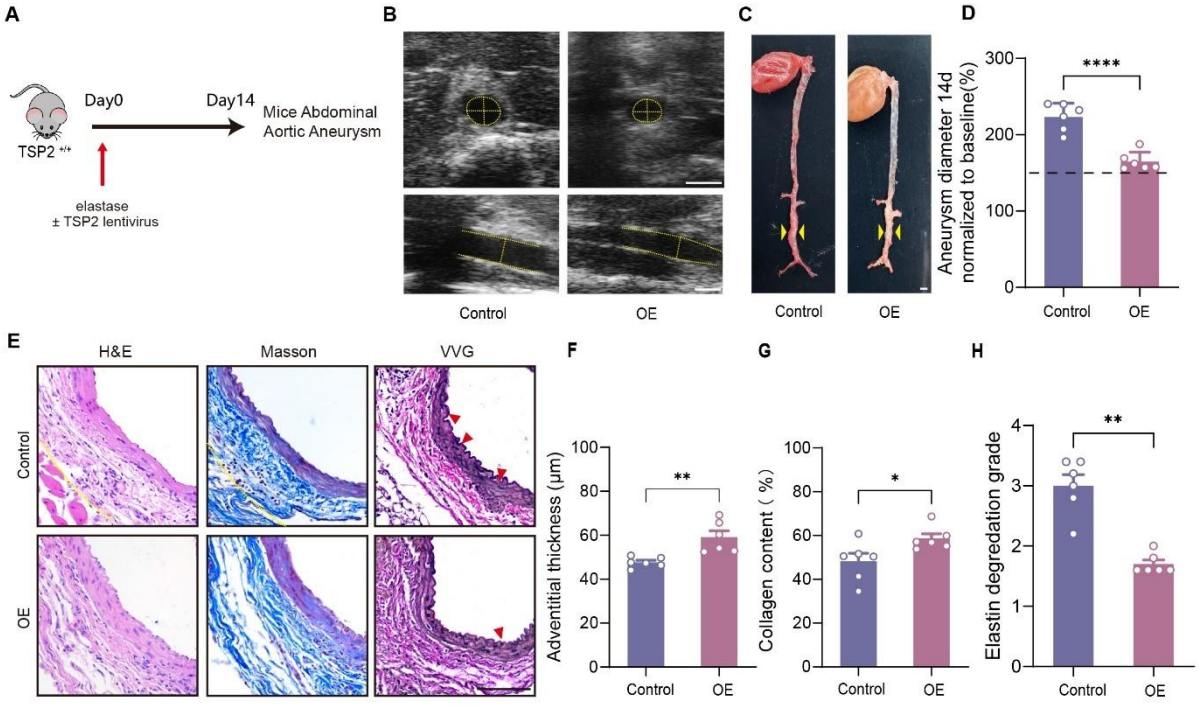

Figure 7: Lentiviral TSP2 Overexpression Attenuates AAA Progression in Wild Type Mice. (A)Experimental design for TSP2$^{+/+}$ mice. Elastase-induced AAA was established in TSP2$^{+/+}$ mice, followed by lentiviral-mediated TSP2 overexpression (OE) or control treatment. Aortic aneurysm analysis was conducted 14 days later. (B) Representative Doppler ultrasound images of the abdominal aorta in TSP2$^{+/+}$ mice treated with (OE) or without (Control) TSP2 overexpression. Yellow dashed lines indicate aneurysm diameter. Scale bars = 1 mm. (C) Gross appearance of the isolated aortas from TSP2$^{+/+}$ mice treated with (OE) or without (Control) TSP2 overexpression, 14 days post-perfusion. Yellow arrowheads indicate aneurysm. Scale bars = 1 mm. (D) Quantification of aneurysm diameter normalized to baseline measurements. TSP2$^{+/+}$ mice overexpressing TSP2 (OE) showed significantly smaller aneurysm diameters compared to controls (n=6). (E) Histological staining of aortic sections from TSP2$^{+/+}$ mice treated with (OE) or without (Control) TSP2 overexpression, including H&E, Masson's trichrome, and VVG staining. Red arrowheads in VVG staining

indicate fragmented elastic fibers. Scale bars = 100μm. (F) Quantification of adventitial thickness from H&E staining. $TSP2^{+/+}$ mice (Control) exhibited significantly reduced adventitial thickness compared to $TSP2^{+/+}$ mice overexpressing TSP2 (OE). (G Collagen content quantified from Masson's trichrome staining, showing significantly higher collagen levels in $TSP2^{+/+}$ mice with TSP2 overexpression (OE) compared to controls (n=6). (H) Elastin degradation grade quantified from VVG staining, showing significantly reduced elastin degradation in $TSP2^{+/+}$ mice with TSP2 overexpression (OE) compared to controls (n=6). Data are shown as mean ± SEM. Statistical significance was determined by unpaired Student's t-test (D, F and G), or Mann-Whitney U test (H).

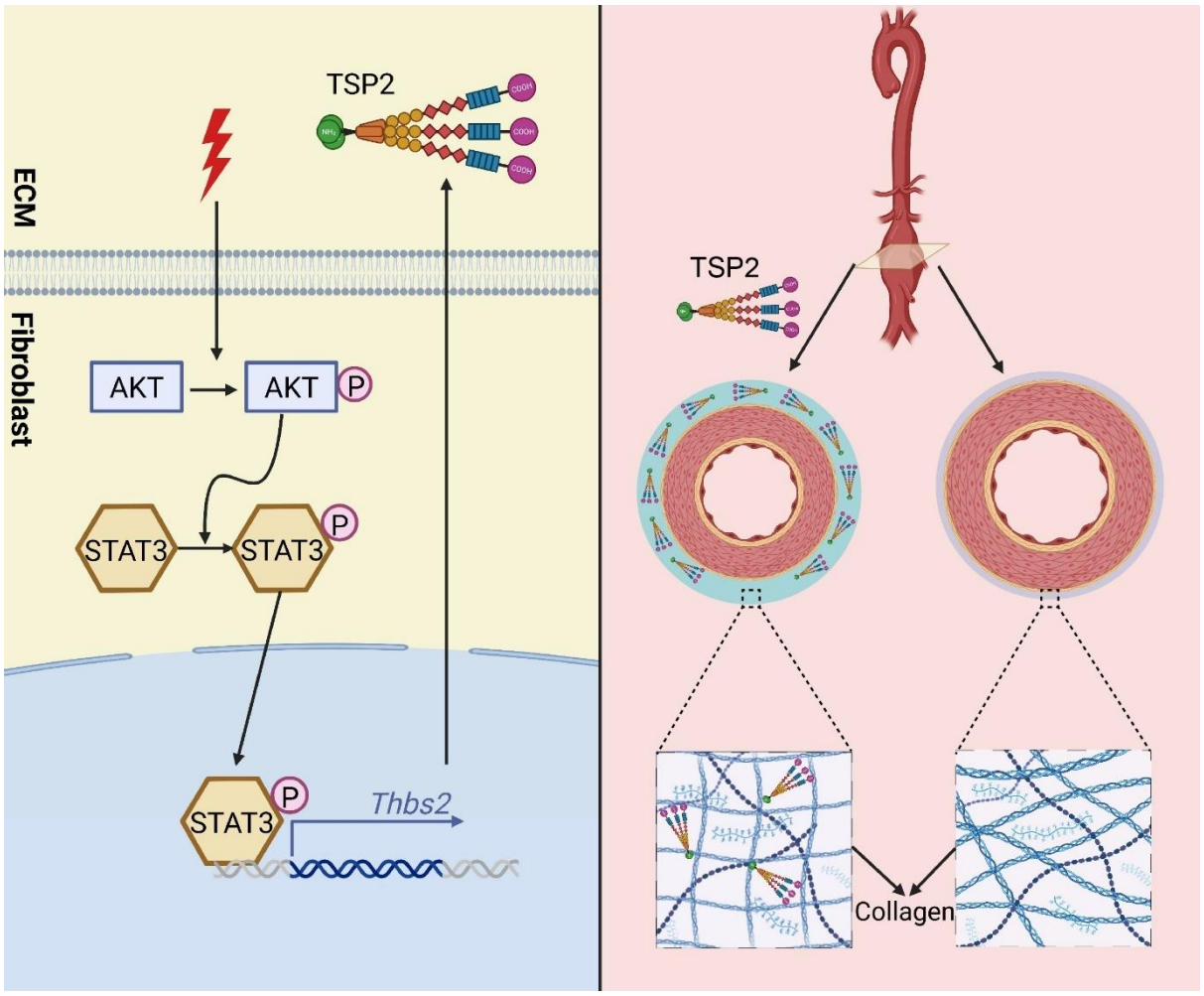

Graphical Abstract